Journal of Environmental Management 381 (2025) 125266

Contents lists available at ScienceDirect

Journal of Environmental Management

journal homepage: www.elsevier.com/locate/jenvman

Research article

Combination of hydrochemical graphical methods and multivariate statistical analysis to delineate groundwater bodies

Stefania Stevenazzi [a,*], Konstantinos Voudouris [b], Daniela Ducci [a]

[a] Università degli Studi di Napoli Federico II, Dipartimento di Ingegneria Civile, Edile e Ambientale, Piazzale Tecchio 80, Naples, 80125, Italy

[b] Aristotle University of Thessaloniki, Department of Structural, Historical & Applied Geology, Laboratory of Engineering Geology & Hydrogeology, University Campus, Thessaloniki, GR54124, Greece

ARTICLE INFO

Handling editor: Lixiao Zhang

Keywords:
Statistical analysis
Groundwater body
Hydrochemistry
Coastal aquifers
Volcanic aquifers
Italy

ABSTRACT

The identification of hydrogeological boundaries and the assessment of the quantitative and qualitative state of groundwater are necessary for the delineation of groundwater bodies, according to the European Guidelines. In this context, this study attempts to verify the current delineation of groundwater bodies (GWBs) focusing on their hydrochemical features through the application of hydrogeochemical methods and multivariate statistical analyses. The areas of interest are three adjacent GWBs located in the north-western sector of Campania Region in Southern Italy: the Volturno-Regi Lagni Plain, a coastal plain constituted of fluvial, pyroclastic and marine sediments; the Plain of Naples, an innermost plain of fluvial and pyroclastic sediments and the Phlegrean Fields, an active volcanic area with a series of monogenic volcanic edifices. Physicochemical data measured in groundwater samples collected at more than 200 sampling points were considered. Results reveal five different hydrogeochemical processes variably influencing the chemical features of the three GWBs: dissolution of carbonate rocks, influence of volcanic deposits and/or gas/hydrothermal fluid upwelling, salinisation, reducing conditions, and anthropogenic contamination. Combining hydrochemical diagrams and multivariate statistical analysis (i.e., factor analysis) allows depicting areas characterised by one or more hydrogeochemical processes, mostly reflecting known processes, but also highlighting the influence of groundwater flowpaths on water chemistry. The current delineation of the three GWBs should be revised considering that some hydrochemical features and processes are peculiar to each GWB, but others are in common between two or more GWBs. Uncertainties in the delineation of GWBs based on their hydrochemical features could be reduced by improving the distribution of the monitoring well network to ensure a more homogeneous coverage.

1. Introduction

The European Guidelines for the delineation of groundwater bodies require the identification of hydrogeological boundaries and the assessment of the quantitative and chemical state of groundwater (EC, 2003; Sánchez et al., 2009). These criteria must ensure that i) a precise estimation of the water budget for each groundwater body and ii) an accurate quantitative and qualitative description of groundwater status can be reliably assessed. Several approaches have been implemented for identifying and delineating groundwater bodies and evaluating their quantitative and qualitative state, following the European Guidelines. These approaches include a combination of geological, stratigraphic and tectonic data (e.g., Szocs et al., 2013; Saroli et al., 2019), also constituting the architecture of geological and hydrostratigraphic models (e.g., Åberg et al., 2021; Stevenazzi et al., 2023), with physicochemical, biological and isotopic data (e.g., Szocs et al., 2013; Brkić et al., 2019; Corniello et al., 2024; Stevenazzi et al., 2023) and groundwater budget evaluation (e.g., Corniello et al., 2024; Petrone et al., 2024), also considering groundwater uses and pressures (e.g., Wada and Heinrich, 2013; De Stefano et al., 2015; Stevenazzi et al., 2023).

Groundwater quality in areas characterised by i) different geological formations (e.g., crystalline vs sedimentary rocks), ii) diversified ecosystems (e.g., wetlands), iii) peculiar geographical patterns (e.g., along the coastline), iv) highly developed human activities (e.g., agricultural and farming activities, industrial and urban areas) may result in heterogeneous hydrochemical facies distribution. Classical graphical methods for aqueous data visualisation, such as Piper (1944), Stiff (1951) and Schoeller (1962), are widely employed for the identification

* Corresponding author.
E-mail address: stefania.stevenazzi@unina.it (S. Stevenazzi).

https://doi.org/10.1016/j.jenvman.2025.125266
Received 6 December 2024; Received in revised form 25 February 2025; Accepted 2 April 2025

of hydrochemical facies, linked to water-rock interaction or mixing-processes (e.g., Tiwari et al., 2019; Doveri et al., 2021; Corniello et al., 2024). However, when dealing with large datasets, these graphical methods have some inherent limitations (Güler et al., 2002). Among statistical methods, multivariate statistical analysis enables the handling of large datasets of chemical and physical parameters for grouping water samples showing similarities into homogeneous clusters (H-mode Cluster Analysis; Güler et al., 2002; Machiwal et al., 2018; Pacheco Castro et al., 2018) or for grouping parameters associated with processes, phenomena or sources based on the structure of the hydrochemical data (R-mode Factor Analysis; Güler et al., 2002; Machiwal et al., 2018; Pacheco Castro et al., 2018). In hydrogeological studies, multivariate statistical analysis has proven to be reliable for the discrimination of groundwaters according to the main withdrawn aquifer, flow paths and potentially inter-aquifer connections (e.g., Panagopoulos et al., 2016; Madrigal-Solís et al., 2022), and the identification of the main hydrochemical processes governing water quality (e.g., Voudouris et al., 2000; Lu et al., 2011; Busico et al., 2018) and their evolution (e.g., Andrade and Stigter, 2009; Parisi et al., 2023; Tziritis et al., 2024). Multivariate statistical analysis constitutes a useful tool for investigating the pollution sources resulting from human activities, such as agricultural or industrial activities directly or indirectly threatening groundwater (e.g., Mfumu Kihumba et al., 2016; Stevenazzi et al., 2020; Crayol et al., 2024; Mali et al., 2024) and for recognising the dynamics of groundwater salinisation largely affecting coastal aquifers (e.g., Yang et al., 2021; Parisi et al., 2023; Crayol et al., 2024; Mali et al., 2024). Multidisciplinary approaches that combine hydrogeological tools (hydrochemical diagrams, bivariate plots, etc.) and multivariate statistical analyses (e.g., principal component analysis, hierarchical cluster analysis, factor analysis) are also employed to facilitate the interpretation of geochemical processes with large hydrochemical data series in geologically complex environments (Kazakis et al., 2017; Ebrahimi et al., 2022; Crayol et al., 2024; Madrigal-Solís et al., 2024).

In this context, this study attempts to verify the current delineation of groundwater bodies (GWBs) through the application of hydrochemical graphical methods and multivariate statistical analysis. The areas of interest are represented by three adjacent GWBs located in the north-western sector of Campania Region (Southern Italy): the Volturno–Regi Lagni Plain, a coastal plain of about 1340 km^2 constituted of fluvial, pyroclastic and marine sediments; the Phlegrean Fields, an active volcanic area constituted of a series of monogenic volcanic edifices; and the Plain of Naples, an inner plain constituted of fluvial and pyroclastic sediments. The identification and delineation of GWBs in Campania Region were developed by the regional public authorities in 2007 (49 GWBs) and updated in 2019 (80 GWBs), in compliance with the European Directives (EC, 2000; Regione Campania, 2019). The basis of the groundwater bodies delineation has been the definition of aquifer groups and their hydrogeological characteristics, using updated geological and hydrogeological maps (De Vita et al., 2018; Regione Campania, 2019; DAM, 2021), enhanced by other datasets (i.e., superficial geology, soil, land use, water quality). The definition has been easy enough in mountainous and hilly areas where there are karstic and volcanic aquifers, often delimited by tectonic lineaments and characterised by constant groundwater flow directions over time. In flat areas, with Quaternary porous deposits, the delineation is a complex task because no clear physical boundaries separate the different geological formations and the different aquifers, that are hydraulically connected. In these situations, groundwater body delineation is mainly based on the groundwater divides identified by the piezometric setting, which also changes over time. Here the hydrochemical profile, and therefore the groundwater quality monitoring, may play a fundamental role in delineating the GWBs.

The main objectives of this study are: i) to identify the main hydrogeochemical processes characterising and affecting the GWBs, by means of hydrochemical facies and statistical analysis of hydrochemical data; ii) to verify the current delineation of the GWBs according to their hydrochemical features and natural or anthropogenic processes affecting them. The study proceeded following the steps: 1) selection of chemical analyses of water samples and compilation of the datasets; 2) application of graphical methods for aqueous data visualisation (classical and colour-coded Piper Diagrams, Stiff Diagrams); 3) grouping of parameters showing similarities based on chemical analyses (R-mode Factor Analysis); 4) mapping of the results of hydrochemical and statistical analyses; 5) identification of hydrochemical features and hydrogeochemical processes; 6) comparison of the results with the current delineation of GWBs.

2. Geographical, geological and hydrogeological setting of the study area

The flat coastal area object of this study is crossed by the Volturno River and is a Quaternary tectonic depression filled by alluvial and volcanic deposits (Romano et al., 1994; Amorosi et al., 2012). The graben, whose subsidence continued over the Quaternary, is surrounded by the Roccamonfina volcano (NE) and by the Mesozoic limestone mountains of the southern Apennines (N and E). In the southern part, the morphology changes in correspondence of the slopes of the Phlegrean Hills consisting of tuffs and pyroclastic deposits. The coastal plain faces the Thyrrenian Sea on the west side.

The area encompasses the groundwater bodies (GWBs) of the Volturno–Regi Lagni Plain (P-VLTR), the Eastern Plain of Naples (P-NAP), and the Phlegrean Fields (FLE), as defined in the River Basin Management Plan 2021–2027 (Regione Campania, 2019; DAM, 2021, Fig. 1). The plain of the P-VLTR GWB (1069 km^2) has been divided in the last River Basin Management Plan into two sectors: the northern sector (P-VLTR$_{DX}$), including the right side of the Volturno River plain, and the southern one (P-VLTR$_{SX}$), including the left side of the Volturno River plain. Both areas consist of shallow discontinuous aquifers and a deeper main aquifer, separated by tuffs (Campanian Ignimbrite, ~39 ky; De Vivo et al., 2001), made up of alluvial, pyroclastic and marine deposits (Fig. 2). The main differences between the two GWBs are in the less human impact in the P-VLTR$_{DX}$ with respect to the P-VLTR$_{SX}$ and in peculiar geochemical characteristics, i.e., negative redox conditions in groundwater in the P-VLTR$_{SX}$ (Corniello and Ducci, 2014; Cuoco et al., 2015b; Busico et al., 2018). The groundwater flow is mainly directed from E to W, from the mountain range towards the seacoast (De Vita et al., 2018, Fig. 1). The stratigraphy and the hydrogeological setting of the Eastern Plain of Naples GWB (430 km^2) are similar to those of the Volturno River Plain (Fig. 2), except in the southern sector, where the tuffs are absent and the aquifer is unique and phreatic, located in the pyroclastic reworked deposits (Corniello and Ducci, 2014; Allocca et al., 2022). The hydrogeological setting of the Phlegrean Fields GWB (203 km^2) is constituted by a succession of pyroclastic layers with different grain sizes and cementation degrees, derived from the various eruption phases of the Phlegrean Fields (Sbrana et al., 2021). The groundwater flow is characterised by a radial pattern directed towards the sea in the south and west, towards the P-VLTR GWB in the north, and towards the P-NAP GWB in the east (Ducci and Sellerino, 2012; De Vita et al., 2018, Fig. 1).

The groundwater depth is 0.5–3 m below ground surface (b.g.s.) in the coastal part and 4–50 m b.g.s. in the rest of the study area. Groundwater natural recharge occurs through direct infiltration of meteoric precipitation, streambed infiltration, and lateral inflows from mountainous area (Allocca et al., 2007; Corniello et al., 2010). In addition, irrigation return flows of applied irrigation water contribute to the recharge of the aquifers. Numerous wells with an average depth of 50 m have been drilled to exploit the aforementioned aquifer systems. The hydrochemical pattern follows the groundwater flow of the plain. The $(Ca^{2+} + Mg^{2+})/(Na^+ + K^+)$ ratio and HCO_3^- content decrease from the limestone mountains to coastal areas, where more alkaline conditions are present (Corniello et al., 2010; Corniello and Ducci, 2014). In the southern part, the hydrogeochemistry is influenced by the closeness

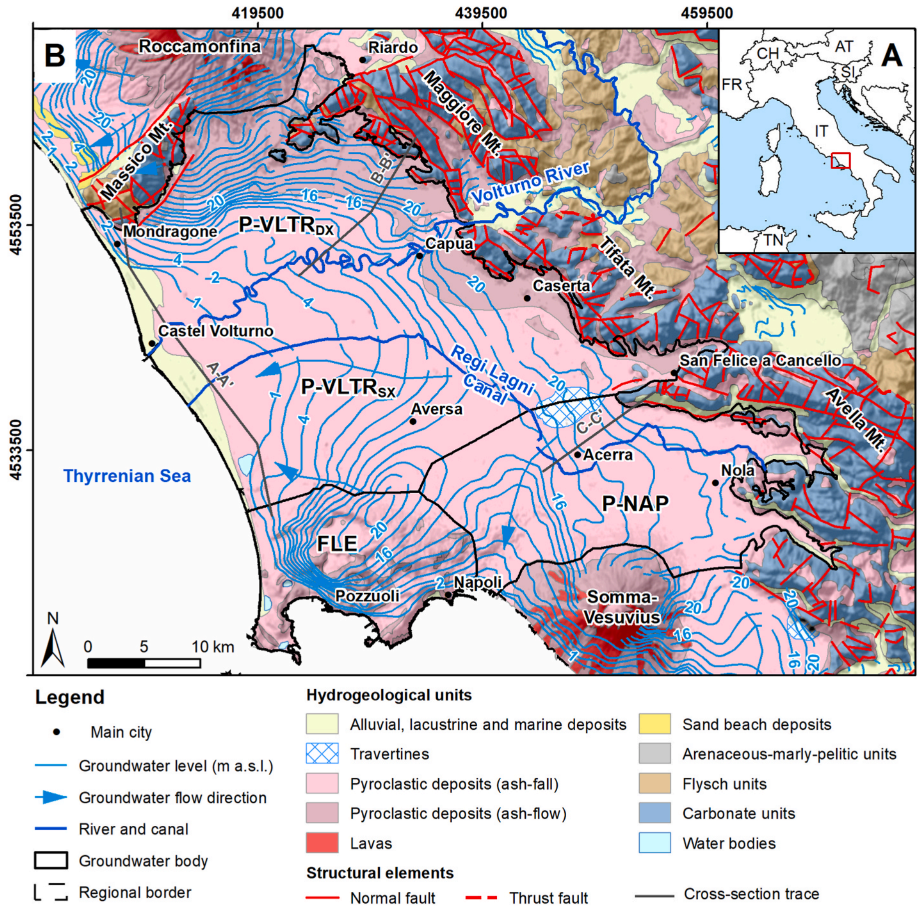

Fig. 1. The study area in the Southern Italy. A) Location of panel B (red frame). FR: France; CH: Switzerland; AT: Austria; SI: Slovenia; IT: Italy; TN: Tunisia. B) Hydrogeological setting of the study area and location of the hydrogeological cross-sections shown in Fig. 2. Piezometric levels, hydrogeological units and structural elements simplified from De Vita et al. (2018). GWBs delineation according to DAM (2021): P-VLTR$_{DX}$ and P-VLTR$_{SX}$ = Volturno-Regi Lagni Plain GWB, right and left sides, respectively; P-NAP = Plain east to Naples GWB; FLE = Phlegrean Fields GWB. Coordinates refer to the WGS 1984—UTM Zone 33 N projection. Basemap: hillshade; source: https://osm-wms.de/.

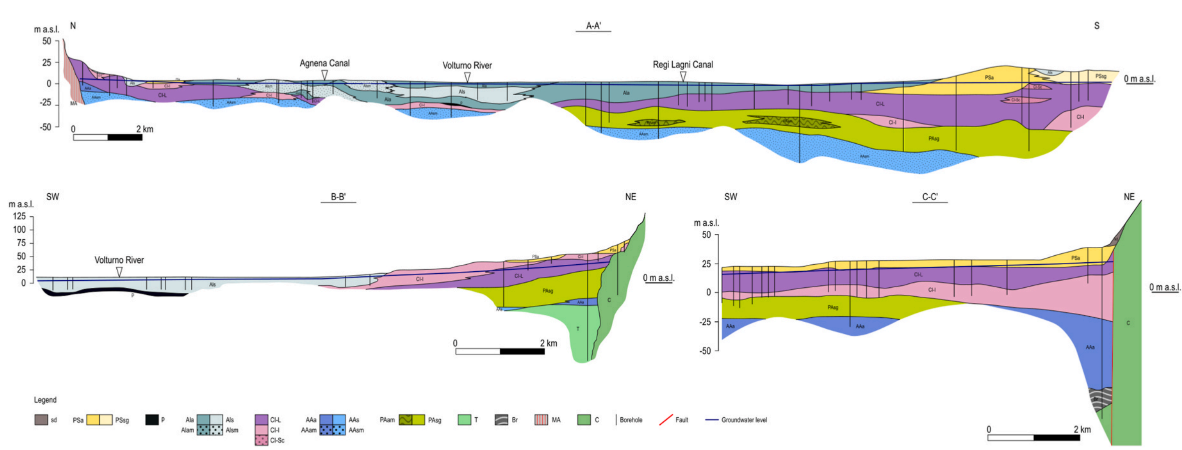

Fig. 2. Simplified hydrogeological cross-sections marked by the black lines on the maps in Fig. 1. Modified from Corniello et al. (2010), Corniello and Ducci (2014), Regione Campania (2004). Legend, from left to right: sd: slope deposits of calcareous debris, sometimes cemented and in a pyroclastic silty sandy matrix; PS: upper pyroclastic deposits of prevalent coarse-sandy (sg) or silty-sandy (a) grain size; p: peat layers; Al: upper alluvial, marshy, lacustrine and marine deposits, clayey and silty (a; am: of marine origin) or sandy (s; sm: of marine origin) grain size; CI: Campanian Ignimbrite, lithoid facies (-L), incoherent facies (-I) and scoriaceous facies (-Sc); AA: lower alluvial and marine deposits, clayey and silty (a; am: of marine origin) or sandy (s; sm: of marine origin) grain size; PA: lower pyroclastic deposits of silty to sand (am: with lenses of marine origin) or coarse-sandy (sg) grain size; T: transitional and marine deposits, fine to coarse grain size; Br: calcareous and calcareous-dolomitic breccias; MA: marly-arenaceous-clayey flysch deposits; C: limestones and dolostones. Groundwater levels from De Vita et al. (2018).

of the Phlegrean Fields, where there is a complex interplay of volcanic and hydrothermal processes (Aiuppa et al., 2003; Allocca et al., 2018). In the whole area, different types of "natural contamination" are observed, especially due to volcanism, such as high fluoride and high arsenic content in groundwater (Corniello and Ducci, 2014; Busico et al., 2018; Sellerino et al., 2019). In the sectors close to the Volturno River, the aquifers present reducing conditions, with low content in sulphate and high Fe and Mn (Corniello and Ducci, 2014; Ducci et al., 2016; Busico et al., 2018). Moreover, there is a widespread contamination by nitrate, predominantly due to intensive agricultural and livestock activities (Cuoco et al., 2015b; Ducci et al., 2019). Seawater intrusion phenomenon occurs not only close to the coastline, but also along the Volturno River, through the ingression of saltwater along the river, and favoured by the medium-high permeable sediments constituting the river channel itself or buried paleochannels (Corniello et al., 2010; Busico et al., 2021; Gaiolini et al., 2023; Colombani et al., 2024).

The climate in Campania Region is affected by rainfall variability depending on the morphology and on the proximity to the Apennines divide, ranging between 700 and 800 mm/y in the coastal and in the eastern sectors of the Region, to almost 2000 mm/y in the mountains, with maximum amount of rainfall in autumn and winter. Mean annual temperatures are about 17–18 °C in the coastal areas, with the hottest period registered in July–August (https://indicatoriambientali.isprambiente.it/).

Since Roman times, thanks to the high fertility of volcanic soils, the economy of the plain has been based on agriculture. Nowadays the main crops in the irrigated arable areas are cereals, legumes and horticulture, followed by permanent crops of fruit trees, olive groves and vineyards (Regione Campania, 2013). In the densely populated sectors (left side of the Volturno River, Phlegrean Hills and eastern Plain of Naples), diversified human activities coexist, including intensive agriculture, grazing, and industrial facilities (CLC, 2018). The northern part of the plain undoubtedly shows less anthropogenic pressure and the prevalent land uses are agricultural fields and livestock farming (CLC, 2018). During the summer, there is an increase in population along the coast due to tourism (Ducci et al., 2017).

3. Material and methods

3.1. Dataset sources and selected hydrochemical parameters

The chemical analyses considered in this study were sourced from different partially or fully publicly available databases (Fig. S1).

- **Database 1:** 172 sampling points; samples collected in 2016–2017; source: data collected in the framework of a collaboration agreement between the Istituto Zooprofilattico Sperimentale del Mezzogiorno (I.Z.S.M.) and the Centro Interdipartimentale di Ricerca 'Ambiente' of the Università degli Studi di Napoli Federico II (C.I.R.AM.) within the framework of "Campania Trasparente – Attività di monitoraggio integrato per la Regione Campania" (Delibera della Giunta Regionale n. 497/2013); unpublished data.
- **Database 2:** 27 sampling points; samples collected in 2013; source: data collected in the framework of the LIFE11/ENV/IT/275ECOR-EMED project "Implementation of Eco-Compatible Protocols for Agricultural Soil Remediation in Litorale Domizio-Agro Aversano NIPS" funded by the European Commission under the LIFE + Programme; data partially published in Ducci et al. (2017).
- **Database 3:** 33 sampling points; samples collected in 2016; source: data collected in the framework of the project "Operational tools for quality assessment and control of agricultural systems in the Campania Plain" funded by the Campania Region; data partially published in Ducci et al. (2019).
- **Database 4:** 30 sampling points; the most recent sample collected in the period 2014–2017 was considered; source: data collected by the Regional Environmental Agency (ARPA Campania) and available online (https://www.arpacampania.it/).
- **Database 5:** 44 sampling points; samples collected in 2019; source: data published in Ebrahimi et al. (2022).

The databases include monitoring point coordinates and sampling date, main physicochemical parameters (temperature, electrical conductivity, pH), major anions and cations, minor and trace elements (e.g., metals) and contaminants (e.g., solvents, pesticides). The hydrochemical datasets include data from public and private wells used for drinking purposes, agricultural, industrial and other (e.g., garden irrigation) activities. Wells intercepting the main aquifer were considered.

Being aware that the long time period (2013–2019) of collected data could be a flaw, the main aim of this study is to represent the groundwater hydrochemical status at the most recent time, considering all the available data covering almost homogeneously and entirely the selected groundwater bodies.

3.2. Quality assurance and data preparation

Data underwent a pre-processing phase for the identification of errors and missing data (Quality Assurance and Quality Control; Hudson et al., 1999; Refsgaard et al., 2010). Below Limit of Detection (LOD) values were replaced by the value of the LOD multiplied by 0.5 (Grath et al., 2001). The parameters with censored or missing values exceeding 20 % were excluded from further statistical analyses. The parameters analysed by only one database were excluded from further statistical analyses.

The physicochemical parameters (electrical conductivity, pH), major cations and anions (Ca^{2+}, Mg^{2+}, Na^{+}, K^{+}, HCO_3^-, Cl^-, SO_4^{2-}, NO_3^-), metalloids (As, B) and some minor elements (F, Fe, Mn, V) were selected. The alkalinity, expressed as mg/L of HCO_3^- was used as an alternative to HCO_3^-. With the HCO_3^- ion predominating in groundwater in the study area (§2), it can be assumed that the errors in anion-cation charge balance could be absorbed by the HCO_3^- ion content. Following this assumption, when the HCO_3^- ion content was missing, it was calculated as the difference between the sum of the cation (Ca^{2+}, Mg^{2+}, Na^{+}, K^{+}) and the sum of the remaining anion (Cl^-, SO_4^{2-}) contents, both expressed as meq/L.

The major ions were used for analytical quality control based on anion−cation charge balance. An anion-cation charge balance error within ±10 % was considered acceptable for samples potentially affected by seawater intrusion (Güler et al., 2002; Parisi et al., 2023). Samples that did not meet the charge balance error were excluded from analyses. A summary table with descriptive statistics of physicochemical parameters and dissolved species included in the databases and passing the pre-processing phase is shown in Table 1.

Following the pre-processing phase described above, the first dataset (**Dataset E**) was built. It includes 232 samples from all the five databases described in §3.1 (Fig. S2A) and ten parameters: Ca^{2+}, Mg^{2+}, Na^{+}, K^{+}, HCO_3^-, Cl^-, SO_4^{2-}, NO_3^-, As, B.

The second dataset (**Dataset H**) was created in order to include two other parameters (Fe and Mn). This choice takes into account the importance of Fe and Mn in characterizing the groundwater chemistry in the study area that was observed in previous studies (§2). These two parameters were not included in **Database 5**. Nonetheless, the percentage of censored values (i.e., below the LOD) for Fe and Mn exceeded the 20 % threshold. For this reason, instead of replacing the censored data, samples showing censored values of Fe and/or Mn were excluded from the dataset. This choice was preferred to avoid a potential exclusion of the parameters in the following statistical analysis. Thus, the dataset includes 114 samples from **Databases 1–4** (Fig. S2B) and 12 parameters: Ca^{2+}, Mg^{2+}, Na^{+}, K^{+}, HCO_3^-, Cl^-, SO_4^{2-}, NO_3^-, As, Fe, Mn, V.

No missing values were present in the datasets.

Table 1
Descriptive statistics of the physicochemical (electrical conductivity, EC; pH) parameters and dissolved species: total number of measures (N), minimum (min), 25th percentile ($P_{0.25}$), median ($P_{0.5}$), 75th percentile ($P_{0.75}$), maximum (max), arithmetic mean (X), standard deviation (s).

Parameter	Unit	N	min	$P_{0.25}$	$P_{0.5}$	$P_{0.75}$	max	X	s
EC	To 20 °C, μS/cm	224	210.0	833.9	1199.5	1622.25	40,000.0	2295.1	5091.8
pH	To 20 °C	224	5.7	6.8	7.0	7.3	8.6	7.1	0.5
As	μg/L	251	0.3	3.0	5.9	16.0	6875.0	107.9	531.8
B	μg/L	250	2.5	25.0	143.0	324.3	88,812.5	1588.5	6830.5
Ca^{2+}	mg/L	251	3.7	79.5	118.0	178.5	710.0	137.3	94.8
Mg^{2+}	mg/L	251	0.1	13.1	26.0	41.7	1704.0	45.8	134.7
Na^{+}	mg/L	251	1.8	53.2	80.0	134.5	13,430.0	425.8	1536.1
K^{+}	mg/L	251	0.4	23.0	41.0	73.0	829.0	68.3	102.6
HCO_3^-	mg/L	251	48.8	353.0	498.0	720.0	15,518.9	639.0	1004.9
Cl^-	mg/L	251	3.3	40.5	77.2	133.0	20,700.0	594.8	2511.0
SO_4^{2-}	mg/L	251	0.1	39.5	75.0	168.5	2980.0	163.3	333.8
NO_3^-	mg/L	237	0.0	5.2	28.0	56.0	355.0	39.7	45.6
F	μg/L	224	0.4	50.0	246.5	967.0	12,000.0	677.4	1168.7
Fe	μg/L	209	3.0	10.0	53.0	503.0	36,800.0	993.6	3355.6
Mn	μg/L	209	0.3	1.0	9.0	205.0	7294.0	386.0	1013.3
V	μg/L	210	0.5	3.4	10.0	14.3	104.0	11.8	13.3

3.3. Classical and alternative hydrochemical data visualisation

The Piper Diagram and its color-coded modification (Piper, 1944; Peeters, 2014) were generated for the visualisation and identification of hydrochemical facies. The Piper Diagram in its colour-coded modification by Peeters (2014) is based on the Hue, Saturation and Value (HSV) colour scheme. A background colour scheme is used to fill the trilinear Piper plot, so that each water sample can be coloured with unique RGB values according to its location in the Piper diagram. By assigning these colours to the sampling locations on maps, a direct link between the sampling location and the Piper plot is established to facilitate the interpretation of hydrochemical data. Yang et al. (2022) improved the colour-coded Piper Diagram by Peeters (2014) by updating the background colour scheme such that it is more perceptually uniform.

RGB values were interpolated by applying the Inverse Distance Weighting (IDW) technique (Shepard, 1968, 1984). The IDW technique assumes that each measured point has a local influence that diminishes with distance. It gives greater weights to points closest to the prediction location, and the weights are proportional to the inverse of the distance raised to the power value. The IDW technique allows to include all observation points in the study area, or to limit the observation points either by means of a specified search radius or by selecting a precise number of known values (Camera et al., 2014). For the interpolation of RGB data, a power value equal to 2 was set, so that the data were inversely weighted as the square of the distance. The number of observations points used for each interpolation was set to 12, as default (Esri, 2025). The three rasters representing red, blue and green colours were combined in a unique raster representing a continuous spatial distribution of the hydrochemical facies as in the colour-coded Piper Diagram. The spatial distribution of the hydrochemical facies was compared with the delineation of the GWBs.

The Stiff Diagrams (Stiff, 1951) for each sample were generated for the visualisation and identification of singular hydrochemical facies that could be masked in the Piper Diagrams, e.g., because of their low representativeness. According to the polygonal shape of the Stiff Diagram, the composition of each water sample was identified and grouped into classes. The spatial distribution of these classes was compared with the spatial distribution of the hydrochemical facies derived from the colour-coded Piper Diagram.

The WQChartPy open-source Python package (Yang et al., 2022) was used for generating the classical and color-coded Piper Diagrams, and the Stiff Diagrams. The spatial interpolations and the combination of RGB bands were performed in ArcGIS (ESRI®) environment. For its completeness, numerosity and areal coverage, **Dataset E** was used in this phase.

3.4. Application of factor analysis and data processing

The R-mode Factor Analysis (FA) was used to reveal latent underlying factors (e.g., key processes, phenomena, sources) that account for the structure of the hydrochemical data (Machiwal et al., 2018). The (hydro)geological interpretation of these factors provides insight into the main processes that may control the spatial distribution of hydrochemical parameters. Mathematically, FA reduces the complexity of the initial data matrix by producing a small number of factors that explain a large amount of the total variance of the raw data (Brown, 1998; Voudouris et al., 2000).

Multivariate statistical analysis (MVSA) techniques are based on the assumptions that data are normally distributed and homoscedastic (have a constant variance over the range of predicted values), in order to ensure meaningful and reliable results (Güler et al., 2002; Machiwal et al., 2018; Helsel et al., 2020). After the pre-processing steps described in §3.2, data underwent normalisation and standardisation of the parameters involved in the analysis. In the first step, the statistical distribution of parameters was checked using the Kolmogorov-Smirnov (K-S) test (Kolmogorov, 1933; Smirnov, 1948). The K-S test is a nonparametric test of the null hypothesis that the population cumulative distribution function (*cdf*) of the data is equal to the hypothesized *cdf* (i.e., normal distribution) (Massey, 1951). Parameters with non-normal distribution were transformed by applying the Box-Cox (Box and Cox, 1964, 1982), the logarithm and the square root transformation. Then, the K-S test was applied on transformed parameters and the best transformation technique was selected according to i) the result of K-S test, either accepting or rejecting the null hypothesis, and ii) the best p-value whether the null hypothesis can be accepted in more than one case (i.e., applying any of the transformation technique). If a parameter showed a non-normal distribution even after any transformation, it was not used in the subsequent statistical analyses. Finally, all parameters displaying a normal distribution were standardized by calculating their standard scores (z-scores), which ensures an equal weight of each parameter in the statistical analysis (Dalton and Upchurch, 1978; Voudouris et al., 1997; Güler et al., 2002).

The Kaiser-Meyer-Olkin (KMO) test was applied to assess the sampling adequacy of the datasets for FA application (Kaiser, 1974, 1981). KMO values higher than 0.5 are considered acceptable, whereas KMO values higher than 0.8–0.9 are considered excellent for FA application (Kaiser, 1974). Principal components analysis was used to obtain the initial factor solution (i.e., factor extraction). Variables showing a value of communalities close to 1 after the extraction are considered reliable in the analysis (Brown, 1998; Voudouris et al., 2000). The number of factors summarising the main processes was selected according to computed eigenvalues and explained variance after the extraction

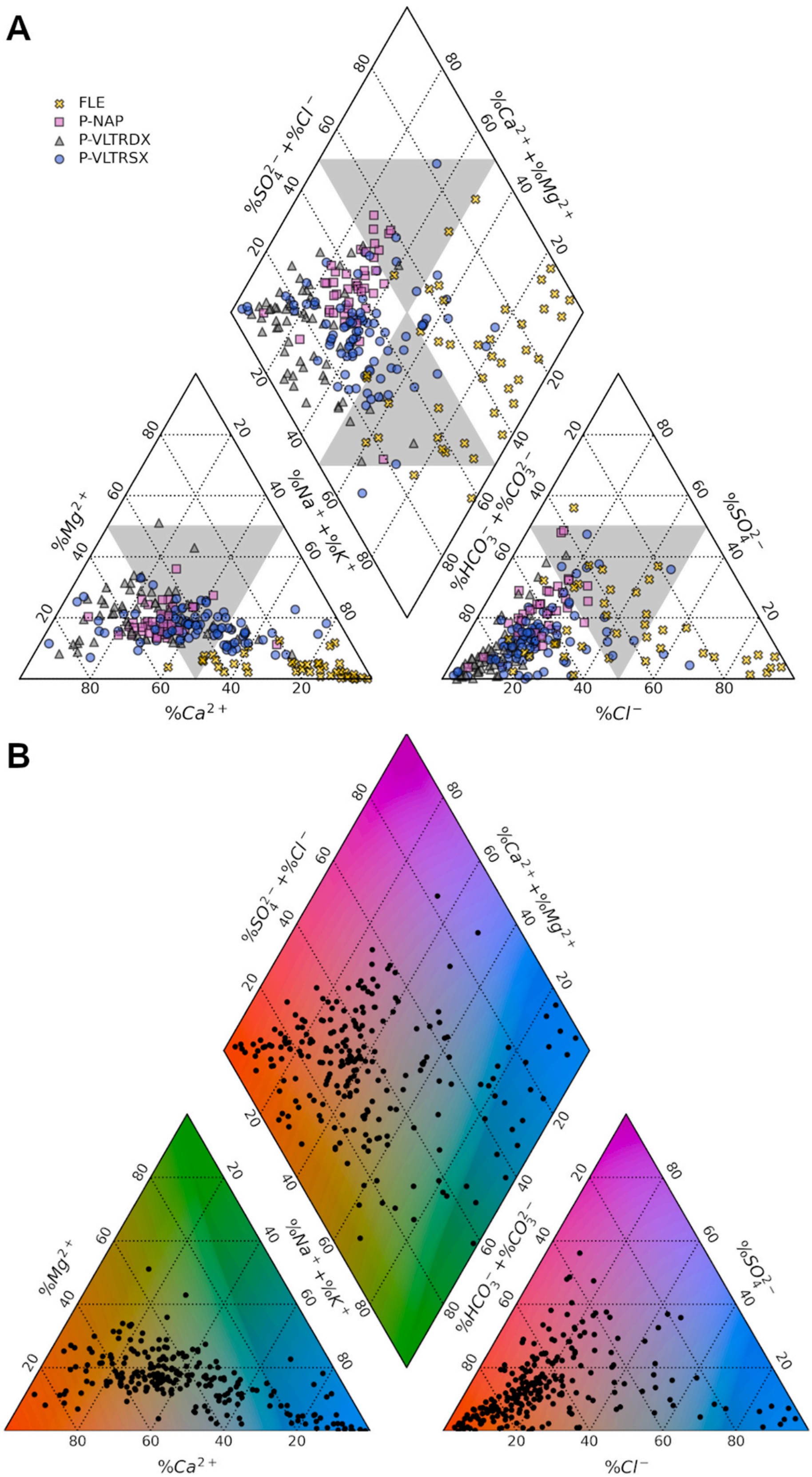

Fig. 3. Classical (a) and colour-coded (b) Piper diagrams. P-VLTR$_{DX}$ and P-VLTR$_{SX}$ = Volturno-Regi Lagni Plain GWB, right and left sides, respectively; P-NAP = Plain east to Naples GWB; FLE = Phlegrean Fields GWB.

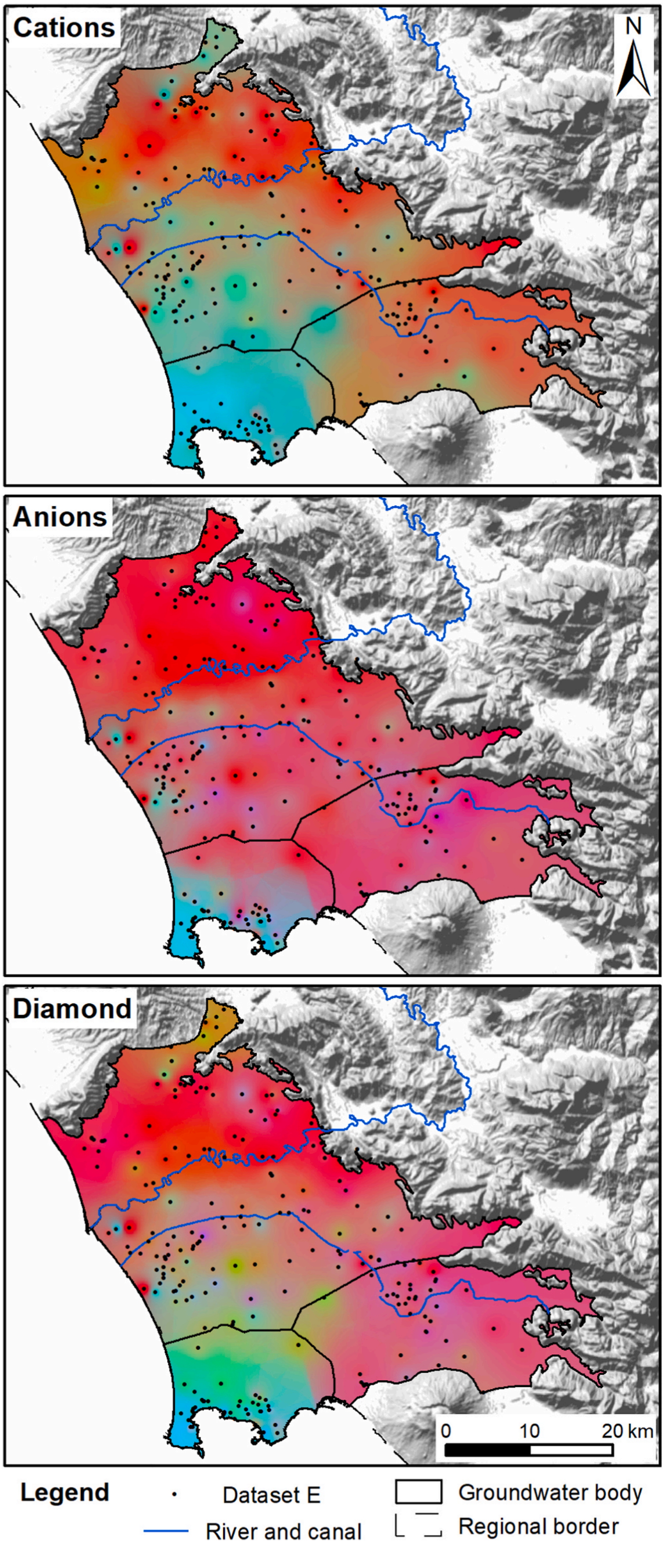

Fig. 4. Colour-coded maps derived from colour-coded Piper diagram (Fig. 3B). GWBs delineation according to DAM (2021). Refer to Fig. 1 for geographical details. Basemap: hillshade; source: https://osm-wms.de/.

(Brown, 1998; Voudouris et al., 2000; Parisi et al., 2023): factors showing eigenvalues higher than 1 were selected. The orthogonal rotation (i.e., varimax) method was applied to minimise the number of variables that have high loadings on each factor, that is to achieve a more accurate interpretation of the results (Kaiser, 1958; Brown, 1998). The factor loading matrix was examined to assess the correlation between each parameter and the factors. The higher the factor loading (close to ± 1), the higher the influence of the parameter on the respective factor. Conversely, factor loadings close to zero indicate a weak correlation between the parameters and the factors (Voudouris et al., 2000; Parisi et al., 2023). In detail, factor loadings with absolute values between 0.75 and 1.0 define a strong correlation; those between 0.5 and 0.75 a moderate one, and those between 0.5 and 0.3 a weak correlation (Ujević Bošnjak et al., 2012; Busico et al., 2018). The geochemical interpretation of factors provides insight of the main processes governing the distribution of hydrochemical variables (Lu et al., 2011; Ujević Bošnjak et al., 2012). Factor scores represent the influence of each factor on the sampling points. Absolute values of factor scores are related to the intensity of the process underlying each factor (Dalton and Upchurch, 1978). Negative values reflect regions not affected by the specific processes each factor represents, whereas positive values indicate areas under the influence of the processes (Voudouris et al., 2000). Maps of the spatial distribution of the factor scores were realised. IDW (§3.3) and kriging (Krige, 1951, 1966; Matheron, 1966) techniques were applied to interpolate factor scores. A power value equal to 2 was set for IDW interpolation. Kriging provides an optimal prediction of an attribute at a target location by minimizing the prediction error variance, assuming that a variogram model is available (Panagiotou et al., 2022). A variogram model and its parameters (sill, range, nugget) were estimated for each factor. In this case, we included all observation points in the study area (Golden Software, 2025). Therefore, the contribution to the estimated value of distant points depended only on the weight for the IDW technique and on the variogram parameters (i.e., range) for the kriging technique. Leave-one-out validation and two skill scores (Nash-Sutcliff coefficient, NSE, and Pearson correlation coefficient, r) were used to evaluate the performance of the interpolation (Hofstra et al., 2008). For each factor, the technique showing the best balance between overall performance and simplicity of computation was used in the following. The resulting maps were compared with the delineation of GWBs.

Data preparation for MVSA, i.e., normalisation and standardisation of parameters, was conducted in Matlab (Mathworks®) environment. R-mode FA was performed in SPSS Statistics (IBM®) environment. The spatial interpolations of factor scores were performed in Surfer (Golden Software®) environment. Both **Dataset E** and **Dataset H** were used in this phase.

4. Results

4.1. Hydrochemical characterisation

The calcium-bicarbonate type is the prevalent hydrochemical facies in the study area, followed by the alkaline-bicarbonate and alkaline-chloride types (Fig. 3A and Fig. S3). From the Piper diagram, the cations present calcium-magnesium ratios higher than 1 with two main clusters: samples from the plain GWBs mainly present either calcium as the dominant cation or none; samples from FLE GWB present alkaline dominant cations. Bicarbonate is the dominant anion in most of the samples, with similar percentages of sulphate and chloride. Very few samples, mainly located in the FLE GWB, show high chloride percentages and low bicarbonate and sulphate.

The Piper Diagram in its colour-coded modification (Fig. 3B) facilitates the interpretation of hydrochemical data, highlighting the transitions between the various hydrochemical facies. Differences in hydrochemical compositions are marked by the transition from red-purple colours to light blue and yellow-green colours in the diamond plot and map (Figs. 3B and 4), reflecting the geological variability of the aquifers within and surrounding the study area, and the changes along the main groundwater flow direction. The calcium-bicarbonate (Ca-HCO_3) facies (red-purple colours) is mainly present in the inner portion of the plain (P-NAP and inner sectors of P-VLTR$_{DX}$ and P-VLTR$_{SX}$ GWBs) and along the coast of P-VLTR$_{DX}$ GWB. In these sectors, the hydrochemistry is affected by groundwater recharge from the carbonate

Table 2
Varimax rotation factor loadings matrix, eigenvalues, total variance explained and communalities for Dataset E. In bold, strong and moderate factor loadings.

Parameter	Factor I	Factor II	Factor III	Communalities
As	**0.875**	−0.148	−0.181	0.820
Ca^{2+}	0.093	**0.920**	0.142	0.876
Mg^{2+}	0.011	**0.904**	−0.023	0.817
K^{+}	**0.861**	0.149	0.134	0.781
HCO_3^-	0.342	**0.763**	−0.282	0.778
Cl^-	**0.869**	0.287	0.080	0.843
SO_4^{2-}	**0.689**	0.301	0.455	0.772
NO_3^-	0.065	−0.089	**0.944**	0.903
Eigenvalue	3.527	1.888	1.176	
Total variance explained (%)	44.1	23.6	14.7	

reliefs surrounding the plain. The alkaline-chloride facies (light blue colour) characterises the FLE GWB, being influenced by the hydrothermal activities of the Phlegrean Fields and seawater intrusion phenomenon. The sodium-chloride (Na-Cl) facies also characterises the coastal area and some inner portions of the P-VLTR$_{SX}$ GWB, suggesting the occurrence of salinisation processes due to seawater intrusion. The alkali-bicarbonate facies is present in the north-eastern corner of the P-VLTR$_{DX}$ GWB, suggesting that the mineralisation process in the aquifer depends on the water-volcanic rock interaction and it is influenced by groundwater recharge from the Roccamonfina volcanic edifice bounding the northern side of the plain (Fig. 1; e.g., Sacchi et al., 2022). Other differences in compositions are highlighted in the cations and anions maps (Fig. 4). In the cations map, alkaline composition (Na^+ and K^+, light blue colours) characterise the FLE and north-eastern corner of the P-VLTR$_{DX}$ GWBs, as shown in the diamond map, but also some inner and coastal sectors of the P-VLTR$_{SX}$ GWB. A slight enrichment in magnesium (yellow-green colours) is present in the north-western corner of the P-VLTR$_{DX}$ GWB, which may be related to localised water-gas (i.e., hydrothermal fluids) and water-rock (i.e., carbonate/volcanic aquifer) interactions (Corniello et al., 2015; Cuoco et al., 2015a). The other sectors are characterised by calcium compositions (dark-to-light red colours), which relative abundance decreases moving away from the carbonate reliefs along the main groundwater flow direction. In the anions map, a peculiar enrichment in bicarbonate (red colour) in the centre of the plain along the Volturno River is evident. An enrichment of chloride (light blue colours) is shown along the coastal sector of the P-VLTR$_{SX}$ and FLE GWBs, strengthening the probable occurrence of the seawater intrusion phenomenon. Strong differences in composition among sampling points located very close to each other are clearly visible in all maps (Fig. 4). This singularity may be due to a point source of contamination, and not to local natural aquifer conditions.

The classification of Stiff Diagrams eases the identification of peculiar and local hydrochemical compositions: ten hydrochemical facies are identified (Fig. S3). It is worth noting that transitional facies are recognised in the middle of the P-VLTR$_{SX}$ GWB (i.e., alkaline- and calcium-bicarbonate facies), where calcium-bicarbonate and alkaline-bicarbonate facies are present on the border with the mountain range and along the coastal sector, respectively. Transitional and highly mixed hydrochemical compositions are abundant in the FLE GWB, highlighting the marked influence of hydrothermal activities of the Phlegrean Fields, which may act locally, and the seawater intrusion phenomenon along the coastline. The hydrochemical facies identified in the P-VLTR$_{DX}$ GWB confirms the results described through the colour-coded Piper Diagram. Sulphate facies (Ca-SO_4 in P-NAP GWB and Na+K-SO_4 in P-VLTR$_{SX}$ GWB) are not visible in the colour-coded maps (Fig. 4), instead they are identified thanks to the Stiff Diagrams (Fig. S3). The presence of SO_4^{2-} and K^+ in groundwater may be due to leaching of agricultural fertilizers, as NPK or $KMgSO_4$ (e.g., Cuoco et al., 2015b; Spoelstra et al., 2021).

4.2. Multivariate statistical analysis

Concerning R-mode FA, some parameters were excluded from **Datasets E and H** because they showed non-normal distribution even after Box-Cox, logarithm or square root transformation, according to the Kolmogorov-Smirnov test. Therefore, B and Na^+ from **Dataset E** and V from **Dataset H** were excluded from the statistical analyses. Results of the factor analysis are shown in Tables 2 and 3 and S1. The variogram model parameters used for the interpolation by means of the kriging technique are reported in Table S2. The performance evaluation of the interpolation techniques used for factor scores and the selected interpolator for each factor/dataset are shown in Table S3.

The R-mode FA on **Dataset E** extracted three factors, which explain 82.4 % of the total variance (Table 2). KMO value is equal to 0.741, therefore the sampling adequacy of the dataset can be considered good. All considered variables show high values of communalities (0.77–0.90), thus they can be considered reliable in the analysis. Factor I accounts for 44.1 % of the total variance of the dataset. It exhibits strong loadings on As, K^+, Cl^- and SO_4^{2-}, and it could be related to several processes occurring at the same time: salinisation due to seawater intrusion (Cl^-), upwelling of hydrothermal fluids in and close to active volcanic areas (As), leaching of organic or mineral fertilisers (K^+, SO_4^{2-}). Positive factor scores (red colours) characterise the southern and south-western portion of the study area, in correspondence of the border with the Somma-Vesuvius volcano, the coastal sector of P-VLTR$_{SX}$ GWB and the entire FLE GWB. Negative factor scores (blue colours) characterise the northern and north-eastern sectors (Fig. 5). Factor II explains 23.6 % of the total variance. It shows strong loadings on Ca^{2+}, Mg^{2+} and HCO_3^-, which are present in groundwater due to dissolution from carbonate rocks (i.e., lateral subsurface recharge from carbonate reliefs surrounding the plain) and derived alluvial materials. Negative factor scores are present in the north-eastern corner of the P-VLTR$_{DX}$ GWB,

Table 3
Varimax rotation factor loadings matrix, eigenvalues, total variance explained and communalities for Dataset H. Extraction forced to obtain four factors. In bold, strong and moderate factor loadings. In italics, not satisfactory values of communalities.

Parameter	Factor I	Factor II	Factor III	Factor IV	Communalities
As	0.200	−0.021	0.262	**0.908**	0.934
Ca^{2+}	−0.066	**0.916**	0.126	−0.018	0.859
Mg^{2+}	0.299	**0.751**	0.331	0.086	0.771
Na^+	0.081	0.136	**0.949**	−0.019	0.926
K^+	−0.206	0.225	0.626	0.241	*0.543*
HCO_3^-	0.493	**0.666**	0.411	−0.086	0.863
Cl^-	−0.076	0.271	**0.764**	0.322	0.766
SO_4^{2-}	**−0.707**	0.522	0.213	0.183	0.850
NO_3^-	**−0.838**	0.046	0.157	−0.171	0.758
Fe	**0.775**	0.207	−0.049	0.002	0.647
Mn	**0.721**	0.281	0.229	0.212	0.696
Eigenvalue	3.940	2.672	1.310	0.692	
Total variance explained (%)	35.8	24.3	11.9	6.3	

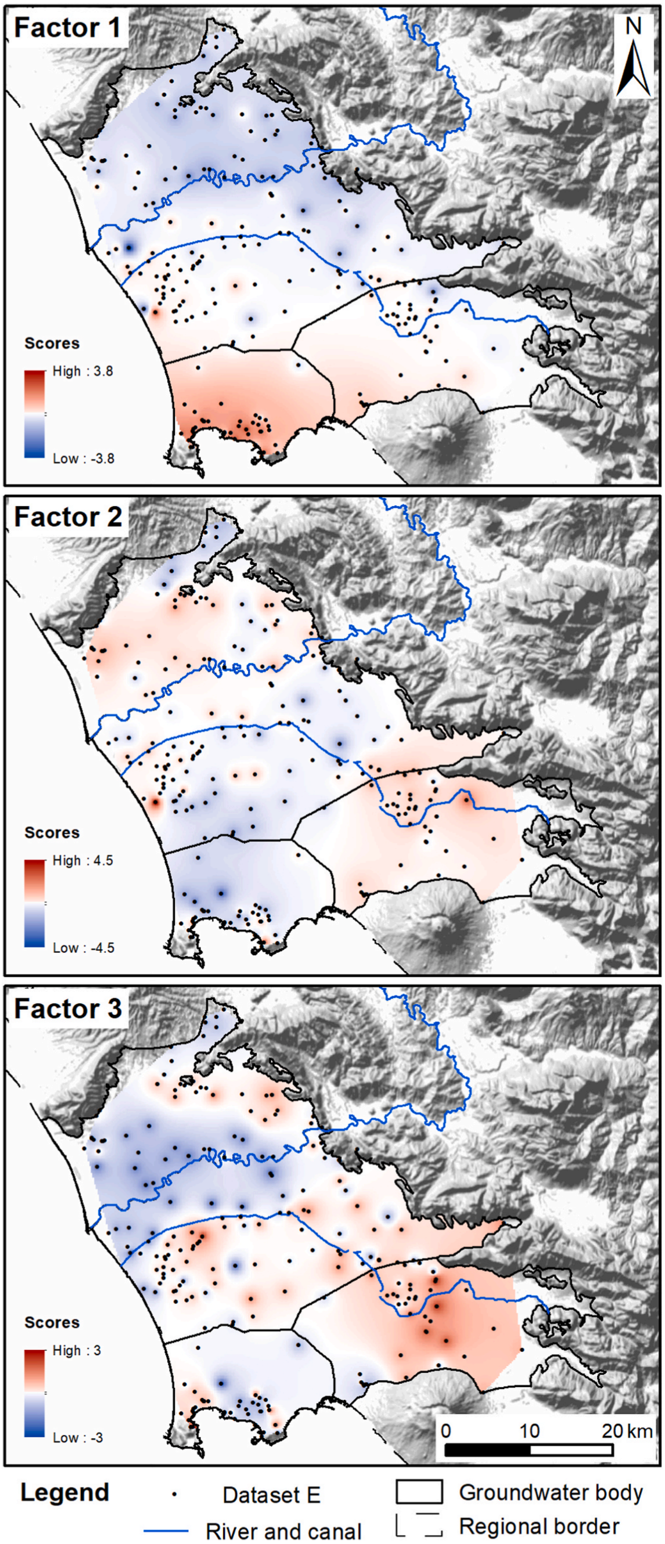

Fig. 5. Spatial distribution of factor scores resulting from FA analysis on Dataset E. GWBs delineation according to DAM (2021). Refer to Fig. 1 for geographical details. Basemap: hillshade; source: https://osm-wms.de/.

close to the Roccamonfina volcano, and in the FLE GWB. Moreover, a large portion of the P-VLTR$_{SX}$ GWB is characterised by negative factor scores. Positive factor scores characterise the sectors of the P-VLTR$_{DX}$ and P-NAP GWBs close to the carbonate reliefs (Fig. 5). Factor III describes 14.7 % of the total variance and it accounts for only one parameter (NO_3^-). Nitrate presence in the studied GWBs derives from human activities related to leakages from sewage systems in urban areas and the leaching of organic and mineral fertilisers in agricultural areas or manure related to livestock activities. Peculiarly, the central area along the Volturno River, pertaining to the P-VLTR$_{DX}$ and P-VLTR$_{SX}$ GWBs, is characterised by negative factor scores. Positive factor scores are present in a large portion of the P-NAP GWB, the southern sector of the P-VLTR$_{SX}$ GWB and in small areas in the FLE and P-VLTR$_{DX}$ GWBs (Fig. 5).

The R-mode FA on **Dataset H** extracted three factors, explaining 72.0 % of the total variance (Table S1). KMO value is equal to 0.571, therefore the sampling adequacy of the dataset can be considered acceptable. Excluding K^+, all the other variables show moderate-to-high values of communalities (0.65–0.85). Factor I explains 35.8 % of the total variance. The factor presents strong positive loadings on five variables (Ca^{2+}, Mg^{2+}, Na^+, HCO_3^-, Cl^-), which could be related to two distinctive hydrochemical processes: salinisation due to seawater intrusion (Na^+, Cl^-) and dissolution from carbonate rocks and derived alluvial materials (Ca^{2+}, Mg^{2+}, HCO_3^-). Factor II accounts for 24.3 % of the total variance. It exhibits strong positive loadings on SO_4^{2-} and NO_3^-, and moderate/strong negative loadings on Fe and Mn. The adverse sign suggests the occurrence of a process that acts opposingly on the two groups of chemical components, either favouring or limiting their dissolution/mobilisation (i.e., reducing conditions). Factor III describes 11.9 % of the total variance and it accounts only one parameter (As). In order to gain more insights of the results, the FA on **Dataset H** was forced to extract more factors, overpassing the eigenvalue criteria. Four factors were extracted, explaining 78.3 % of the total variance (Table 3). Also in this case, K^+ is excluded from the interpretation of the results because of the low value of communalities. Factor I explains 35.8 % of the total variance. It exhibits negative loadings on SO_4^{2-} and NO_3^-, and positive loadings on Fe and Mn. The geographical distribution of this factor overlays the distribution of Factor 3 extracted from **Dataset E**. The central area along the Volturno River is characterised by positive factor scores, therefore connected to the presence of Fe and Mn in groundwater. Negative factor scores are present in a large portion of the P-NAP GWB, the southern sector of the P-VLTR$_{SX}$ GWB close to the Regi Lagni canal and in small areas in the P-VLTR$_{DX}$ GWBs, therefore related to the presence of SO_4^{2-} and NO_3^- in groundwater (Fig. 6). Factor II shows 24.3 % of the total variance and accounts for Ca^{2+}, Mg^{2+}, and HCO_3^-. The combination of these three ions represents the dissolution of carbonate rocks (i.e., lateral subsurface recharge) and derived alluvial materials. Unexpectedly, the distribution of positive factor scores does not follow the border of the study area with the carbonate reliefs, especially in the central sector of the Volturno Plain (Fig. 6). Factor III accounts for 11.9 % of the total variance. It shows strong loadings on Na^+ and Cl^-, which are present in groundwater due to aquifer salinisation, mainly related to the presence of shallow marine sediments (e.g., in the proximity of the Volturno River mouth) together with the actual seawater intrusions. Positive factor scores characterise the coastal sector of the P-VLTR$_{SX}$ GWB and some inner sectors of the P-VLTR$_{SX}$, P-NAP and FLE GWBs. The P-VLTR$_{DX}$ GWB is characterised by negative factor scores (Fig. 6). Factors II and III present the variables aggregated into Factor I obtained following the eigenvalue criteria. Therefore, forcing the analysis to extract more factors allowed distinguishing the processes affecting their occurrence in groundwater. Factor IV describes 6.3 % of the total variance and it accounts only one parameter (As). As presence in groundwater is related to the upwelling of hydrothermal fluids in and close to active volcanic areas. Positive factor scores are present in the P-NAP GWB on the border with the Somma-Vesuvius volcano and in the north-western and north-eastern corners of the P-VLTR$_{DX}$ GWB. Negative factor scores mainly characterise the sectors close to the carbonate reliefs (Fig. 6).

5. Discussion

The Piper Diagram in its colour-coded modification facilitated the

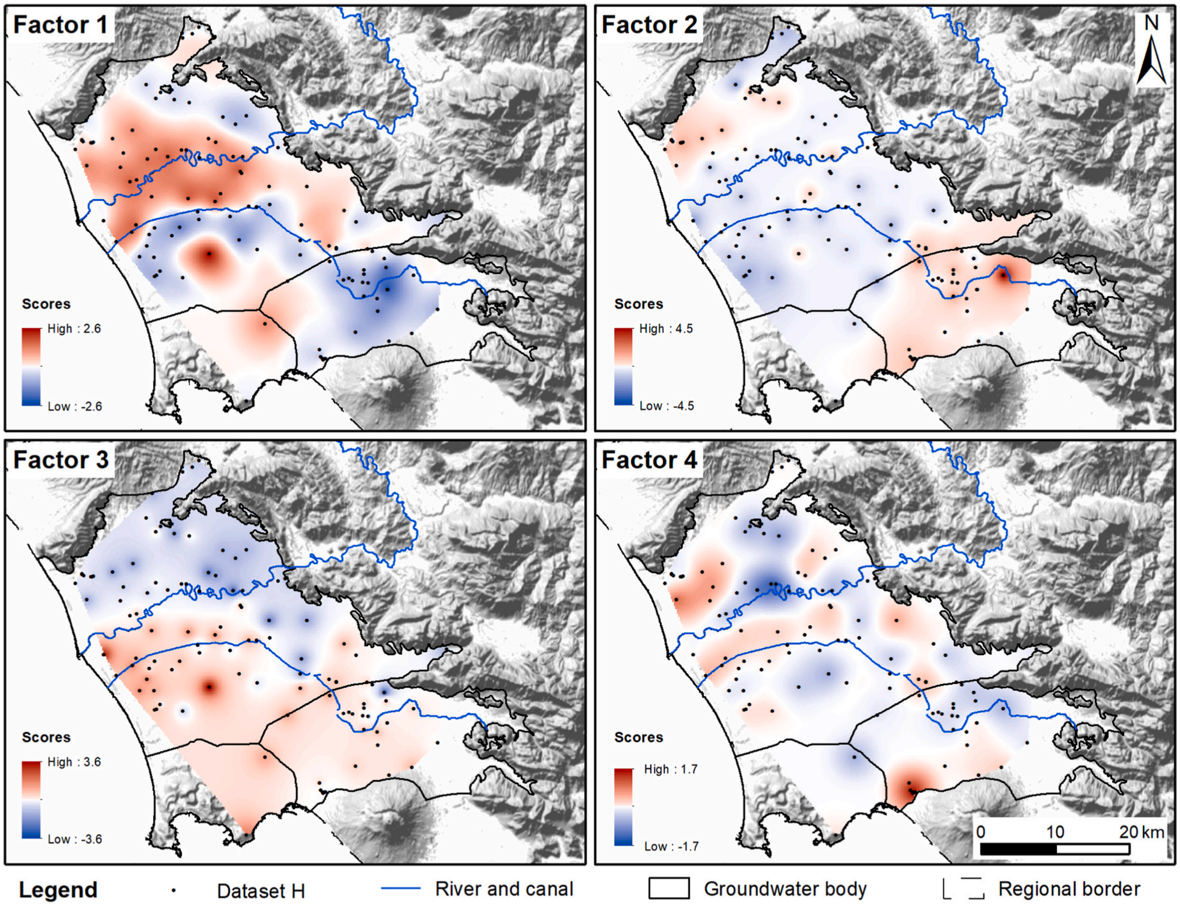

Fig. 6. Spatial distribution of factor scores resulting from FA analysis on Dataset H. GWBs delineation according to DAM (2021). Refer to Fig. 1 for geographical details. Basemap: hillshade; source: https://osm-wms.de/.

interpretation of hydrochemical composition, highlighting seamless transitions between the various hydrochemical facies. R-mode FA enabled identifying the different processes characterising the hydrogeochemistry of the studied aquifer. The comparison of the resulting maps reveals five different hydrogeochemical processes: i) dissolution of carbonate rocks (Ca^{2+}, Mg^{2+}, HCO_3^-); lithology of volcanic deposits and/or influence of gas/hydrothermal fluid upwelling (Mg^{2+}, Na^+, K^+, As); iii) salinisation (Na^+, Cl^-); iv) reducing conditions (HCO_3^-, Fe, Mn); v) anthropogenic contamination impacts (SO_4^{2-}, NO_3^-). These processes have already been recognised in hydrogeological studies that considered samples collected in various sampling campaigns in the study area (e.g., Corniello et al., 2010; Corniello and Ducci, 2014; Cuoco et al., 2015b; Allocca et al., 2018; Busico et al., 2018; Ducci et al., 2019; Mastrocicco et al., 2021; Ebrahimi et al., 2022; Sacchi et al., 2022; Cocca et al., 2024; Corniello et al., 2024).

The influence of the carbonate rocks, that is the prevalence of Ca^{2+}, Mg^{2+} and HCO_3^- ions released from the carbonate aquifer that laterally recharge the plains, decreases along the groundwater flow direction from the mountainous reliefs to the coastline, which is clear for P-$VLTR_{DX}$ and P-NAP GWBs. Instead, the influence of the subsurface recharge from the carbonate rocks is unexpectedly less evident on the eastern border of the P-$VLTR_{SX}$ GWB (Factor 2 in Figs. 5 and 6). In parallel, the progressive enrichment in Na^+ and K^+ ions along the groundwater flow direction is due to leaching and/or ion exchange processes occurring in the pyroclastic-alluvial materials of the plain (Fig. 4). This pattern is masked in Figs. 5 and 6 (Factor 1 and 4, respectively) by the more pronounced influence of hydrothermal fluid upwelling occurring in active volcanic areas as the Phlegrean Fields (FLE GWB), or close to the volcanic edifices of Somma-Vesuvius (southern border of the P-NAP GWB) and Roccamonfina (north-eastern corner of the P-$VLTR_{DX}$ GWB). Several extensive faults characterise the border between the plain and the mountainous reliefs, which favour CO_2 upwelling locally enhancing the mobilisation of alkali ions and metals (e. g., in correspondence of Maggiore and Avella Mts.; Corniello, 1996). This feature is recognised in localised enrichments in ions (Ca^{2+}, Mg^{2+}, HCO_3^-), e.g., between the cities of Acerra and Nola along the Regi-Lagni Canal in P-NAP GWB (Factor 2 in Figs. 5 and 6). The combination of both carbonate and volcanic rocks interaction with groundwater and deep fluids or gases upwelling is particularly evident in P-$VLTR_{DX}$ GWB, in correspondence of the cities of Mondragone and Riardo. The first sector is characterised by an enrichment in Mg^{2+} and As, the second by Na^+, K^+ and As (Fig. 4 and Factor 4 in Fig. 6).

Salinisation occurs along the coast of P-$VLTR_{SX}$ and FLE GWBs, and partially along the Volturno River in $VLTR_{DX}$ GWB (Factor 3 in Fig. 6). Salinisation along the coast of $VLTR_{DX}$ GWB may be masked by the lateral groundwater recharge from the carbonate/marly relief of Massico Mt. enriched in Ca^{2+}, Mg^{2+} and HCO_3^- (Factor 2 in Fig. 6). Salinisation along the coast is related to the seawater intrusion phenomenon, which occurs not only near the coast, but also along the Volturno River, through the ingression of saltwater along the river, and favoured by the medium-high permeable sediments constituting the river channel itself or buried paleochannels (Corniello et al., 2010; Busico et al., 2018). Recent local studies revealed that actual seawater intrusion could not be the main driver for groundwater salinisation at the Volturno River mouth: Colombani et al. (2024) proposed a combined process, including trapped paleo-seawater and redox related processes occurring in peat layers, as responsible for the widespread groundwater salinity. The occurrence of Na^+ and Cl^- in groundwater in inner sectors of FLE, P-NAP and P-VLTR$_{SX}$ GWBs overlaps the occurrence of As (Factor 3 and 4 in Fig. 6). Therefore, their combined presence is related to gases or hydrothermal fluids upwelling, previously described.

A reducing environment is recognised by the combined presence in groundwater of HCO_3^-, Fe and Mn, and the absence SO_4^{2-} and NO_3^-, in the central sector of the Volturno plain, along the Volturno River itself affecting both the P-VLTR$_{DX}$ GWB and the P-VLTR$_{SX}$ GWB (Fig. 4, Factor 3 in Fig. 5 and Factor 1 in Fig. 6). Reducing conditions are established by the confined/semi-confined nature of the aquifer and the enrichment in organic matter in the subsoil due to the presence of clay and peat layers (Fig. 2). Therefore, a reducing environment favours the mobilisation of Fe and Mn, commonly contained in minerals of igneous origin (Hem, 1985), as in the volcanic deposits constituting the aquifer, and an increase in alkalinity (i.e., bicarbonate content). Moreover, denitrification processes are favoured in a reducing environment (Rivett et al., 2008), as established by the low NO_3^- content despite the prevalence of agricultural land use in the plain. The pressure posed by human activities affects all the GWBs (red colours represented in Factor 3 in Fig. 5 and blue colours in Factor 1 in Fig. 6), with the exceptions due to the prevalence of other dominant processes, such as reducing environments or deep fluid upwelling. Leakages from sewage systems in urban areas and leaching of organic and mineral fertilisers in agricultural areas or manure related to livestock activities are mainly responsible for SO_4^{2-} and NO_3^- occurrence in groundwater (Menció et al., 2016; Kaushal et al., 2020), although N and S atmospheric depositions cannot be neglected (Sutton et al., 2011; Stevenazzi et al., 2020; Nunziata, 2023).

The identification of hydrogeochemical features and processes indicates that the current delineation of GWBs does not completely reflect the distribution of peculiar hydrochemical features. The FLE GWB is the only one characterised by the prevalence of one process affecting the hydrochemistry of the entire GWB (i.e., volcanic activity). However, the extension of this process is biased by the scarcity of monitoring points located on the border with the other GWBs. Salinisation and anthropogenic contamination also occur in this GWB, but only in small areas along the coastline. The P-NAP GWB is naturally characterised by calcium-bicarbonate water and affected by anthropogenic pressures, due to the presence of urban areas and agricultural fields. A small influence of volcanic activity occurs on the edge with the Somma-Vesuvius volcano. The western sector of the P-NAP GWB lacks monitoring points. P-VLTR$_{DX}$ and P-VLTR$_{SX}$ GWBs are characterised by several natural processes, due to the intrinsic features of the aquifer, groundwater recharge from mountainous reliefs bordering the plain, gas/fluid upwelling associated with hydrothermal activity or extensive regime, and groundwater salinisation. Reducing conditions affect both GWBs along the border represented by the Volturno River. Apparently, groundwater salinisation less affects the P-VLTR$_{DX}$ GWBs with respect to the P-VLTR$_{SX}$ GWBs; however, this could be masked by other processes or biased by the lack of sampling points along the coastline. These GBWs are also affected by anthropogenic pressures, mainly due to the presence of agricultural fields and livestock activities, which release fertilisers and manure that affect groundwater quality, and indirectly enhance seawater intrusion or saline water movement through aquifer overexploitation along the coast.

Therefore, attention should be given when selecting monitoring points for the assessment of the quality status of GWBs to accomplish with EU Directives. The reconstruction of a suitable conceptual model of the GWB enable the assessment of the impact of the pollutants in the GWB, as well as potentially transferred to groundwater dependent ecosystems or surface water bodies (e.g., rivers, wetlands), the extent of any saline intrusion in the GWB, and the risk for human consumption, accomplishing with EU Directives (EC, 2000; EC, 2006).

It is worth to mention the drawbacks of this study and some methodological issues that have been observed. Stiff Diagrams are useful for depicting peculiar hydrochemical compositions. However, interpreting large datasets can be time-consuming, and dilemmas may arise when working with low-mineralized samples. Carefulness should be posed in the interpretation of colour-coded maps derived from colour-coded Piper Diagrams, because colours may be distorted due to spatial interpolation of RGB bands. Moreover, the spatial interpolation by means of the IDW technique can be biased by the amount of data and non-homogenous distribution of sampling points. This aspect is particularly evident in the southern sector of the study area (FLE GWB), where most of the sampling points are concentrated along the coast. Conversely, the IDW technique enabled recognising peculiar hydrochemical compositions associated to local conditions (e.g., point sources of contamination), instead of natural aquifer conditions. Similarly, the spatial interpolation of factor scores is influenced by the amount of data and non-homogeneous distribution of sampling points, considering both Dataset E and H. The indices of performance highlight that in most of the cases the interpolation is satisfactory, but a few cases present nearly acceptable results (F2-E, F4-H). We point out that these factors do not represent the same process.

The datasets considered in this study cover several years of monitoring activity. Although not mandatory for GWBs delineation (EC, 2003), a stricter approach would require to analyse only data collected during the same sampling campaign. This flaw was considered acceptable for the purpose of this study. Overall, the proposed approach remains useful for an evaluation of the delineation and the assessment of a hydrochemical conceptual model of the GWBs.

6. Conclusions

The paper presents a methodology for the evaluation of the correct delineation of groundwater bodies according to their hydrochemical features based on the joint use of hydrochemical diagrams and multivariate statistical analysis. The key findings can be summarised as follows.

- Hydrogeochemical features and processes were depicted for each GWB, including the influence of carbonate rocks and volcanic rocks, hydrothermal fluids and gases upwelling, reducing environments, anthropogenic contamination, salinisation and seawater intrusion.
- Water chemistry is influenced by the groundwater flowpaths, i.e., a gradual transition from calcium-bicarbonate to alkaline-bicarbonate and alkaline-chloride facies occurs from the mountainous range to the coast.
- Some features and processes are peculiar to one GWB (e.g., hydrothermal fluids upwelling in FLE GWB), whereas others are common to two GWBs (e.g., reducing environment along the Volturno River between P-VLTR$_{DX}$ and P-VLTR$_{SX}$ GWBs).
- The presence of a well-distributed network of monitoring wells with sufficient water quality data is a necessary requirement for an appropriate delineation of GWBs. Currently, a lack of observation points causes uncertainties in the correct delineation of hydrochemical features and processes along the borders of GWBs (e.g., along the coastline, at the edge of the Phlegrean Fields).

In conclusion, the results of this and previous studies on the hydrochemical features of the studied groundwater bodies should be considered in the next review of the River Basin Management Plan, in compliance with the European requirements of the Water Framework Directive 2000/60/EC and Groundwater Directive 2006/118/EC. Specifically, a proposal to review the delineation of the three GWBs could contemplate that.

- The Volturno River currently represents the border between P-VLTR$_{DX}$ and P-VLTR$_{SX}$ GWBs, however several processes affect groundwater quality, both along the river itself and, especially, in correspondence of its mouth. Therefore, the area affected by processes connected to the present and past dynamics of the Volturno River represents a singularity in the plain.

- Fluid and gas upwelling influences the general water chemistry in localised areas along the border with the carbonate mountainous range of P-VLTR and P-NAP GWBs, e.g., close to the Roccamonfina volcano or along the Apennines range due to an extensive regime. Hence, future planning of water resources should consider the localised occurrence of mineralized waters.
- The uncertainties in the extension of the area affected by the hydrothermal and volcanic activity of the Phlegrean Fields, and therefore of the boundaries of the FLE GWBs, could be reduced by improving the distribution of the monitoring well network.
- Groundwater salinisation and seawater intrusion phenomena threaten the coastal sector of P-VLTR and FLE GWBs, potentially worsening a significant portion of agricultural land in the plain. Therefore, investigating the source and the extension of groundwater salinity in this area is crucial for developing effective strategies to protect groundwater resources.

As pointed out by Sánchez et al. (2009), a balance between the requirements and criteria set out in the European Directives and the guidance documents, and a rational and effective water management strategy is necessary to identify and delineate GWBs, avoiding the fragmentation of the aquifers into many small water bodies, but merging smallest groundwater bodies to others of the same nature and the same state. Therefore, previous and large geological and hydrogeological knowledge is essential to delimitate groundwater bodies correctly.

Finally, the peculiar geological aspects and, therefore, the characteristic groundwater chemistry should be considered in planning the water quality monitoring network to ensure a reliable assessment of the groundwater quality status of the groundwater bodies, in compliance with the European regulations.

CRediT authorship contribution statement

Stefania Stevenazzi: Writing – review & editing, Writing – original draft, Visualization, Validation, Software, Methodology, Formal analysis, Data curation, Conceptualization. **Konstantinos Voudouris:** Writing – review & editing, Validation, Supervision, Methodology, Conceptualization. **Daniela Ducci:** Writing – review & editing, Validation, Supervision, Resources, Methodology, Funding acquisition, Conceptualization.

Declaration of competing interest

The authors declare that they have no known competing financial interests or personal relationships that could have appeared to influence the work reported in this paper.

Acknowledgments

The research conducted by Stefania Stevenazzi is supported by the Italian Ministry of University and Research in the framework of the National Operational Programme Research & Innovation 2014–2020 - Axis IV, "Education and research for recovery - REACT-EU" (Università degli Studi di Napoli Federico II: CUP E65F21003160003). The authors would like to thank the two anonymous reviewers who helped to improve the manuscript.

Appendix A. Supplementary data

Supplementary data to this article can be found online at https://doi.org/10.1016/j.jenvman.2025.125266.

Data availability

Data will be made available on request.

References

Åberg, S.C., Åberg, A.K., Korkka-Niemi, K., 2021. Three-dimensional hydrostratigraphy and groundwater flow models in complex Quaternary deposits and weathered/fractured bedrock: evaluating increasing model complexity. Hydrogeol. J. 29, 1043–1074. https://doi.org/10.1007/s10040-020-02299-4.

Aiuppa, A., D'Alessandro, W., Federico, C., Palumbo, B., Valenza, M., 2003. The aquatic geochemistry of arsenic in volcanic groundwaters from southern Italy. In: Applied Geochemistry, Arsenic Geochemistry-Selected Papers from the 10th Water-Rock Interaction Symposium, pp. 1283–1296. https://doi.org/10.1016/S0883-2927(03)00051-9. Villasimius, Italy, 10-15 June 2001 18.

Allocca, V., Celico, F., Celico, P., De Vita, P., Fabbrocino, S., Mattia, C., Monacelli, G., Musilli, I., Piscopo, V., Scalise, A.R., Summa, G., Tranfaglia, G., 2007. Hydrogeological Map of Southern Italy. Istituto Poligrafico e Zecca dello Stato, Roma.

Allocca, V., Coda, S., De Vita, P., Di Rienzo, B., Ferrara, L., Giarra, A., Mangoni, O., Stellato, L., Trifuoggi, M., Arienzo, M., 2018. Hydrogeological and hydrogeochemical study of a volcanic-sedimentary coastal aquifer in the archaeological site of Cumae (Phlegraean Fields, southern Italy). J. Geochem. Explor. 185, 105–115. https://doi.org/10.1016/j.gexplo.2017.11.004.

Allocca, V., Coda, S., Calcaterra, D., De Vita, P., 2022. Groundwater rebound and flooding in the Naples' periurban area (Italy). J. Flood Risk Manag. 15, e12775. https://doi.org/10.1111/jfr3.12775.

Amorosi, A., Pacifico, A., Rossi, V., Ruberti, D., 2012. Late Quaternary incision and deposition in an active volcanic setting: the Volturno valley fill, southern Italy. Sediment. Geol., 2011 Tohoku-oki tsunami 282, 307–320. https://doi.org/10.1016/j.sedgeo.2012.10.003.

Andrade, A.I.A.S.S., Stigter, T.Y., 2009. Multi-method assessment of nitrate and pesticide contamination in shallow alluvial groundwater as a function of hydrogeological setting and land use. Agric. Water Manag. 96, 1751–1765. https://doi.org/10.1016/j.agwat.2009.07.014.

Box, G.E., Cox, D.R., 1964. An analysis of transformations. J. R. Stat. Soc. Ser. B 26, 211–252. https://doi.org/10.1111/j.2517-6161.1964.tb00553.x.

Box, G.E., Cox, D.R., 1982. An analysis of transformations revisited, rebutted. J. Am. Stat. Assoc. 77 (377), 209–210. https://doi.org/10.1080/01621459.1982.10477788.

Brkić, Ž., Kuhta, M., Larva, O., Gottstein, S., 2019. Groundwater and connected ecosystems: an overview of groundwater body status assessment in Croatia. Environ. Sci. Eur. 31, 75. https://doi.org/10.1186/s12302-019-0261-6.

Brown, C.E., 1998. Applied Multivariate Statistics in Geohydrology and Related Sciences. Springer, Berlin, Heidelberg. https://doi.org/10.1007/978-3-642-80328-4.

Busico, G., Cuoco, E., Kazakis, N., Colombani, N., Mastrocicco, M., Tedesco, D., Voudouris, K., 2018. Multivariate statistical analysis to characterize/discriminate between anthropogenic and geogenic trace elements occurrence in the Campania Plain, Southern Italy. Environ. Pollut. 234, 260–269. https://doi.org/10.1016/j.envpol.2017.11.053.

Busico, G., Buffardi, C., Ntona, M.M., Vigliotti, M., Colombani, N., Mastrocicco, M., Ruberti, D., 2021. Actual and forecasted vulnerability assessment to seawater intrusion via GALDIT-SUSI in the Volturno River mouth (Italy). Remote Sens. 13, 3632. https://doi.org/10.3390/rs13183632.

Camera, C., Bruggeman, A., Hadjinicolaou, P., Pashiardis, S., Lange, M.A., 2014. Evaluation of interpolation techniques for the creation of gridded daily precipitation (1 × 1 km2); Cyprus, 1980–2010. J. Geophys. Res. Atmos. 119, 693–712. https://doi.org/10.1002/2013JD020611.

Regione Campania, 2004. Piano di tutela delle acque. Il Contributo Al Piano Di Tutela Delle Acque Della Regione Campania. SELCA, Firenze.

Regione Campania, 2013. Il territorio rurale della Campania. Un viaggio nei sistemi agroforestali della regione attraverso i dati del 6° Censimento Generale dell'Agricoltura. Imago Editrice srl – Dragoni (CE) 450. ISBN: 978-88-95230-24-5. http://www.agricoltura.regione.campania.it/pubblicazioni/pdf/territorio_rurale.pdf. (Accessed 2 September 2024).

CLC, 2018. CORINE Land Cover 2018 vector data for the Italian territory. Available at: https://groupware.sinanet.isprambiente.it/uso-copertura-e-consumo-di-suolo/library/copertura-del-suolo/corine-land-cover. (Accessed 2 September 2024).

Cocca, D., Stevenazzi, S., Ducci, D., Luca, D.A.D., Lasagna, M., 2024. Spatio-temporal variability of groundwater hydrochemical features in different hydrogeological settings in Piedmont and Campania regions (Italy), a comparative study. Acque Sotterranee - Ital. J. Groundw. 13, 29–45. https://doi.org/10.7343/as-2024-748.

Colombani, N., Alessandrino, L., Gaiolini, M., Gervasio, M.P., Ruberti, D., Mastrocicco, M., 2024. Unravelling the salinity origins in the coastal aquifer/aquitard system of the Volturno River (Italy). Water Res. 263, 122145. https://doi.org/10.1016/j.watres.2024.122145.

Corniello, A., 1996. Lineamenti idrogeochimici dei principali massicci carbonatici della Campania. Memor. Soc. Geol. Ital. 51, 333–342.

Corniello, A., Ducci, D., 2014. Hydrogeochemical characterization of the main aquifer of the "Litorale Domizio-Agro Aversano NIPS" (Campania — southern Italy). J. Geochem. Explor. 137, 1–10. https://doi.org/10.1016/j.gexplo.2013.10.016.

Corniello, A., Ducci, D., Trifuoggi, M., Rotella, M., Ruggieri, G., 2010. Hydrogeology and hydrogeochemistry of the plain between Mt. Massico and the River Volturno (Campania regione, Italy). Ital. J. Eng. Geol. Environ. 1, 51–64. https://doi.org/10.4408/IJEGE.2010-01.O-04.

Corniello, A., Cardellicchio, N., Cavuoto, G., Cuoco, E., Ducci, D., Minissale, A., Mussi, M., Petruccione, E., Pelosi, N., Rizzo, E., Polemico, M., Tamburino, S., Tedesco, D., Tiano, P., Iorio, M., 2015. Hydrogeological characterization of a geothermal system: the case of the thermo-mineral area of Mondragone (Campania, Italy). Int. J. Environ. Res. 9, 523–534. https://doi.org/10.22059/ijer.2015.926.

Corniello, A., Ducci, D., Stellato, L., Stevenazzi, S., Massaro, L., Del Gaudio, E., 2024. Combining groundwater budget, hydrochemistry and environmental isotopes to identify the groundwater flow in carbonate aquifers located in Campania Region (Southern Italy). J. Hydrol.: Reg. Stud. 53, 101790. https://doi.org/10.1016/j.ejrh.2024.101790.

Crayol, E., Huneau, F., Garel, E., Zuffianò, L.E., Limoni, P.P., Romanazzi, A., Mattei, A., Re, V., Knoeller, K., Polemio, M., 2024. Investigating pollution input to coastal groundwater-dependent ecosystems in dry Mediterranean agricultural regions. Sci. Total Environ. 954, 176015. https://doi.org/10.1016/j.scitotenv.2024.176015.

Cuoco, E., Darrah, T.H., Buono, G., Eymold, W.K., Tedesco, D., 2015a. Differentiating natural and anthropogenic impacts on water quality in a hydrothermal coastal aquifer (Mondragone Plain, Southern Italy). Environ. Earth Sci. 73, 7115–7134. https://doi.org/10.1007/s12665-014-3892-3.

Cuoco, E., Darrah, T.H., Buono, G., Verrengia, G., De Francesco, S., Eymold, W.K., Tedesco, D., 2015b. Inorganic contaminants from diffuse pollution in shallow groundwater of the Campanian Plain (Southern Italy). Implications for geochemical survey. Environ. Monit. Assess. 187, 46. https://doi.org/10.1007/s10661-015-4307-y.

Dalton, M.G., Upchurch, S.B., 1978. Interpretation of hydrochemical facies by factor analysis. Groundwater 16, 228–233. https://doi.org/10.1111/j.1745-6584.1978.tb03229.x.

DAM, 2021. Piano di gestione delle acque ciclo 2021-2027. Autorità di Bacino Distrettuale dell'Appennino Meridionale. https://www.distrettoappenninomeridionale.it/piano-gestione-acque/iii-ciclo-2021-2027/. (Accessed 2 September 2024).

De Stefano, L., Fornés, J.M., López-Geta, J.A., Villarroya, F., 2015. Groundwater use in Spain: an overview in light of the EU water framework directive. Int. J. Water Resour. Dev. 31, 640–656. https://doi.org/10.1080/07900627.2014.938260.

De Vita, P., Allocca, V., Celico, F., Fabbrocino, S., Mattia, C., Monacelli, G., Musilli, I., Piscopo, V., Scalise, A.R., Summa, G., Tranfaglia, G., Celico, P., 2018. Hydrogeology of continental southern Italy. J. Maps 14, 230–241. https://doi.org/10.1080/17445647.2018.1454352.

De Vivo, B., Rolandi, G., Gans, P.B., Calvert, A., Bohrson, W.A., Spera, F.J., Belkin, H.E., 2001. New constraints on the pyroclastic eruptive history of the Campanian volcanic Plain (Italy). Mineral. Petrol. 73, 47–65. https://doi.org/10.1007/s007100170010.

Doveri, M., Natali, S., Franceschi, L., Menichini, M., Trifirò, S., Giannecchini, R., 2021. Carbonate aquifers threatened by legacy mining: hydrodynamics, hydrochemistry, and water isotopes integrated approach for spring water management. J. Hydrol. 593, 125850. https://doi.org/10.1016/j.jhydrol.2020.125850.

Ducci, D., Sellerino, M., 2012. Natural background levels for some ions in groundwater of the Campania region (southern Italy). Environ. Earth Sci. 67, 683–693. https://doi.org/10.1007/s12665-011-1516-8.

Ducci, D., de Melo, M.T.C., Preziosi, E., Sellerino, M., Parrone, D., Ribeiro, L., 2016. Combining natural background levels (NBLs) assessment with indicator kriging analysis to improve groundwater quality data interpretation and management. Sci. Total Environ. 569–570, 569–584. https://doi.org/10.1016/j.scitotenv.2016.06.184.

Ducci, D., Albanese, S., Boccia, L., Celentano, E., Cervelli, E., Corniello, A., Crispo, A., De Vivo, B., Iodice, P., Langella, C., Lima, A., Manno, M., Palladino, M., Pindozzi, S., Rigillo, M., Romano, N., Sellerino, M., Senatore, A., Speranza, G., Fiorentino, N., Fagnano, M., 2017. An integrated approach for the environmental characterization of a wide potentially contaminated area in southern Italy. Int. J. Environ. Res. Publ. Health 14, 693. https://doi.org/10.3390/ijerph14070693.

Ducci, D., Del Gaudio, E., Sellerino, M., Stellato, L., Corniello, A., 2019. Hydrochemical and isotopic analyses to identify groundwater nitrate contamination. The alluvial-pyroclastic aquifer of the Campanian plain (southern Italy). Geoingegneria Ambientale e Mineraria 156, 5–13.

Ebrahimi, P., Guarino, A., Allocca, V., Caliro, S., Avino, R., Bagnato, E., Capecchiacci, F., Carandente, A., Minopoli, C., Santi, A., Albanese, S., 2022. Hierarchical clustering and compositional data analysis for interpreting groundwater hydrogeochemistry: the application to Campi Flegrei volcanic aquifer (south Italy). J. Geochem. Explor. 233, 106922. https://doi.org/10.1016/j.gexplo.2021.106922.

Esri, 2025. How inverse distance weighted interpolation works. https://pro.arcgis.com/en/pro-app/latest/help/analysis/geostatistical-analyst/how-inverse-distance-weighted-interpolation-works.htm. (Accessed 13 February 2025).

European Commission, 2000. Directive 2000/60/EC of the European parliament and of the council of 23 october 2000 establishing a framework for community action in the field of water policy. Offic. J. Eur. Commun. 22 December 2000, L 327/1-72.

European Commission, 2003. WFD CIS Guidance Document No. 2. Identification of Water Bodies. Published by the Directorate General Environment of the European Commission, Brussels. ISBN No. 92-894-5122-X, ISSN No. 1725-1087.

European Commission, 2006. Directive 2006/118/EC of the European Parliament and of the Council of 12 December 2006 on the protection of groundwater against pollution and deterioration. Off. J. Eur. Union 31, 27 December 2006, L 372/19.

Gaiolini, M., Colombani, N., Mastrocicco, M., Postacchini, M., 2023. Seawater intrusion assessment along the Volturno River (Italy) via numerical modeling and spectral analysis. J. Hydrol. 626, 130289. https://doi.org/10.1016/j.jhydrol.2023.130289.

Golden Software, 2025. No search. https://surferhelp.goldensoftware.com/griddata/search_type.htm. (Accessed 13 February 2025).

Grath, J., Scheidleder, A., Uhlig, S., Weber, K., Kralik, M., Keimel, T., Gruber, D., 2001. The EU water framework directive: statistical aspects of the identification of groundwater pollution trends, and aggregation of monitoring results. In: Final Report. Austrian Federal Ministry of Agriculture and Forestry, Environment and Water Management (Ref.: 41.046/01eIV1/00 and GZ 16 2500/2-I/6/00), European Commission (Grant Agreement Ref.: Subv 99/130794), in Kind Contributions by Project Partners. Vienna, Austria. Available at: https://circabc.europa.eu/sd/a/a1f194ce-8684-436c-a130-ec88ee781bd2/Groundwater%20trend%20report.pdf. (Accessed 16 September 2024).

Güler, C., Thyne, G.D., McCray, J.E., Turner, K.A., 2002. Evaluation of graphical and multivariate statistical methods for classification of water chemistry data. Hydrogeol. J. 10, 455–474. https://doi.org/10.1007/s10040-002-0196-6.

Helsel, D.R., Hirsch, R.M., Ryberg, K.R., Archfield, S.A., Gilroy, E.J., 2020. Statistical Methods in Water Resources. U.S. Geological Survey Techniques and Methods, p. 458. https://doi.org/10.3133/tm4a3 book 4, chap. A3.

Hem, J.D., 1985. Study and interpretation of the chemical characteristics of natural water. U.S. Geological Survey. https://doi.org/10.3133/wsp2254.WaterSupplyPaper2254.

Hofstra, N., Haylock, M., New, M., Jones, P., Frei, C., 2008. Comparison of six methods for the interpolation of daily, European climate data. J. Geophys. Res. Atmos. 113. https://doi.org/10.1029/2008JD010100.

Hudson, H.R., McMillan, D.A., Pearson, C.P., 1999. Quality assurance in hydrological measurement. Hydrol. Sci. J. 44, 825–834. https://doi.org/10.1080/02626669909492276.

Kaiser, H.F., 1958. The varimax criterion for analytic rotation in factor analysis. Psychometrika 23, 187–200. https://doi.org/10.1007/BF02289233.

Kaiser, H.F., 1974. An index of factorial simplicity. Psychometrika 39, 31–36. https://doi.org/10.1007/BF02291575.

Kaiser, H.F., 1981. A revised measure of sampling adequacy for factor-analytic data matrices. Educ. Psychol. Meas. 41, 379–381. https://doi.org/10.1177/001316448104100216.

Kaushal, S.S., Wood, K.L., Galella, J.G., Gion, A.M., Haq, S., Goodling, P.J., Haviland, K.A., Reimer, J.E., Morel, C.J., Wessel, B., Nguyen, W., Hollingsworth, J.W., Mei, K., Leal, J., Widmer, J., Sharif, R., Mayer, P.M., Newcomer Johnson, T.A., Newcomb, K.D., Smith, E., Belt, K.T., 2020. Making 'chemical cocktails' – evolution of urban geochemical processes across the periodic table of elements. Appl. Geochem. 119, 104632. https://doi.org/10.1016/j.apgeochem.2020.104632.

Kazakis, N., Mattas, C., Pavlou, A., Patrikaki, O., Voudouris, K., 2017. Multivariate statistical analysis for the assessment of groundwater quality under different hydrogeological regimes. Environ. Earth Sci. 76, 349. https://doi.org/10.1007/s12665-017-6665-y.

Kolmogorov, A.N., 1933. Sulla determinazione empirica di una legge di distribuzione. Giornale dell'Istituto Italiano degli Attuari 4, 83–91.

Krige, D.G., 1951. A Statistical Approach to Some Basic Mine Valuation Problems on the Witwatersrand, 52. Journal of the Southern African Institute of Mining and Metallurgy, pp. 119–139. https://doi.org/10.10520/AJA0038223X_4792.

Krige, D.G., 1966. Two-dimensional Weighted Moving Average Trend Surfaces for Ore Evaluation, 66. Journal of South African Institute of Mining and Metallurgy, pp. 13–38.

Lu, K.-L., Liu, C.-W., Wang, S.-W., Jang, C.-S., Lin, K.-H., Liao, V.H.-C., Liao, C.-M., Chang, F.-J., 2011. Assessing the characteristics of groundwater quality of arsenic contaminated aquifers in the Blackfoot disease endemic area. J. Hazard Mater. 185, 1458–1466. https://doi.org/10.1016/j.jhazmat.2010.10.069.

Machiwal, D., Cloutier, V., Güler, C., Kazakis, N., 2018. A review of GIS-integrated statistical techniques for groundwater quality evaluation and protection. Environ. Earth Sci. 77, 681. https://doi.org/10.1007/s12665-018-7872-x.

Madrigal-Solís, H., Jiménez-Gavilán, P., Vadillo-Pérez, I., Fonseca-Sánchez, A., Calderón-Sánchez, H., Quesada-Hernández, L., Gómez-Cruz, A., 2022. Discriminant model and hydrogeochemical processes for characterizing preferential flow paths in four interconnected volcanic aquifers in Costa Rica. Hydrogeol. J. 30, 2315–2340. https://doi.org/10.1007/s10040-022-02557-7.

Madrigal-Solís, H., Vadillo-Pérez, I., Jiménez-Gavilán, P., Fonseca-Sánchez, A., Quesada-Hernández, L., Calderón-Sánchez, H., Gómez-Cruz, A., Murillo, J.H., Salazar, R.P., 2024. A multidisciplinary approach using hydrogeochemistry, δ15NNO3 isotopes, land use, and statistical tools in evaluating nitrate pollution sources and biochemical processes in Costa Rican volcanic aquifers. Sci. Total Environ. 951, 174996. https://doi.org/10.1016/j.scitotenv.2024.174996.

Mali, M., Alfio, M.R., Balacco, G., Ranieri, G., Specchio, V., Fidelibus, M.D., 2024. Mobility of trace elements in a coastal contaminated site under groundwater salinization dynamics. Sci. Rep. 14, 24859. https://doi.org/10.1038/s41598-024-75974-1.

Massey, F.J., 1951. The Kolmogorov-Smirnov test for goodness of fit. J. Am. Stat. Assoc. 46 (253), 68–78. https://doi.org/10.2307/2280095.

Mastrocicco, M., Gervasio, M.P., Busico, G., Colombani, N., 2021. Natural and anthropogenic factors driving groundwater resources salinization for agriculture use in the Campania plains (Southern Italy). Sci. Total Environ. 758, 144033. https://doi.org/10.1016/j.scitotenv.2020.144033.

Matheron, G., 1966. Principles of geostatistics. Econ. Geol. 58, 1246–1266.

Menció, A., Mas-Pla, J., Otero, N., Regàs, O., Boy-Roura, M., Puig, R., Bach, J., Domènech, C., Zamorano, M., Brusi, D., Folch, A., 2016. Nitrate pollution of groundwater; all right…, but nothing else? Sci. Total Environ. 539, 241–251. https://doi.org/10.1016/j.scitotenv.2015.08.151.

Mfumu Kihumba, A., Ndembo Longo, J., Vanclooster, M., 2016. Modelling nitrate pollution pressure using a multivariate statistical approach: the case of Kinshasa groundwater body, Democratic Republic of Congo. Hydrogeol. J. 24, 425–437. https://doi.org/10.1007/s10040-015-1337-z.

Nunziata, G.P., 2023. Trace-elements monitoring of single rainwaters for the environmental risks assessment in the "Land of Fires" located between the provinces of Naples and Caserta. Environ. Earth Sci. 82, 186. https://doi.org/10.1007/s12665-023-10868-5.

Pacheco Castro, R., Pacheco Ávila, J., Ye, M., Cabrera Sansores, A., 2018. Groundwater quality: analysis of its temporal and spatial variability in a karst aquifer. Groundwater 56, 62–72. https://doi.org/10.1111/gwat.12546.

Panagiotou, C.F., Kyriakidis, P., Tziritis, E., 2022. Application of geostatistical methods to groundwater salinization problems: a review. J. Hydrol. 615, 128566. https://doi.org/10.1016/j.jhydrol.2022.128566.
Panagopoulos, G.P., Angelopoulou, D., Tzirtzilakis, E.E., Giannoulopoulos, P., 2016. The contribution of cluster and discriminant analysis to the classification of complex aquifer systems. Environ. Monit. Assess. 188, 591. https://doi.org/10.1007/s10661-016-5590-y.
Parisi, A., Alfio, M.R., Balacco, G., Güler, C., Fidelibus, M.D., 2023. Analyzing spatial and temporal evolution of groundwater salinization through multivariate statistical analysis and hydrogeochemical facies evolution-diagram. Sci. Total Environ. 862, 160697. https://doi.org/10.1016/j.scitotenv.2022.160697.
Peeters, L., 2014. A background color scheme for piper plots to spatially visualize hydrochemical patterns. Groundwater 52, 2–6. https://doi.org/10.1111/gwat.12118.
Petrone, P., De Vita, P., Marsiglia, P., Allocca, P., Coda, S., Cusano, D., Lepore, D., Allocca, V., 2024. Hydrogeological conceptual model and groundwater recharge of Avella Mts. karst aquifer (southern Italy): a literature review and update. J. Hydrol.: Reg. Stud. 54, 101871. https://doi.org/10.1016/j.ejrh.2024.101871.
Piper, A.M., 1944. A graphic procedure in the geochemical interpretation of water-analyses. Trans. Am. Geophys. Union 25 (6), 914–923.
Refsgaard, J.C., Højberg, A.L., Møller, I., Hansen, M., Søndergaard, V., 2010. Groundwater modeling in integrated water resources management—visions for 2020. Groundwater 48, 633–648. https://doi.org/10.1111/j.1745-6584.2009.00634.x.
Regione Campania, 2019. Piano di Tutela delle Acque della Regione Campania. https://www.regione.campania.it/regione/it/tematiche/acque/piano-di-tutela-delle-acque-2020-2026-j872?page=1. (Accessed 2 September 2024).
Rivett, M.O., Buss, S.R., Morgan, P., Smith, J.W.N., Bemment, C.D., 2008. Nitrate attenuation in groundwater: a review of biogeochemical controlling processes. Water Res. 42, 4215–4232. https://doi.org/10.1016/j.watres.2008.07.020.
Romano, P., Santo, A., Voltaggio, M., 1994. L'evoluzione geomorfologica della pianura del Fiume Volturno (Campania) durante il tardo Quaternario (Pleistocene medio-superiore - Olocene). Il Quaternario Italian Journal of Quaternary Sciences 7 (1/a), 41–56.
Sacchi, E., Cuoco, E., Oster, H., Paolucci, V., Tedesco, D., Viaroli, S., 2022. Tracing groundwater circulation in a valuable mineral water basin with geochemical and isotopic tools: the case of FERRARELLE, Riardo basin, Southern Italy. Environ. Geochem. Health 44, 1–28. https://doi.org/10.1007/s10653-021-00845-x.
Sánchez, D., Carrasco, F., Andreo, B., 2009. Proposed methodology to delineate bodies of groundwater according to the European water framework directive. Application in a pilot Mediterranean river basin (Málaga, Spain). J. Environ. Manag. 90 (3), 1523–1533. https://doi.org/10.1016/j.jenvman.2008.11.001.
Saroli, M., Lancia, M., Petitta, M., 2019. The geology and hydrogeology of the Cassino plain (central Apennines, Italy): redefining the regional groundwater balance. Hydrogeol. J. 27, 1563–1579. https://doi.org/10.1007/s10040-019-01953-w.
Sbrana, A., Marianelli, P., Pasquini, G., 2021. The Phlegrean Fields volcanological evolution. J. Maps 17, 557–570. https://doi.org/10.1080/17445647.2021.1982033.
Schoeller, H., 1962. Les Eaux Souterraines. Mason et Cie, Paris.
Sellerino, M., Forte, G., Ducci, D., 2019. Identification of the natural background levels in the Phlaegrean fields groundwater body (Southern Italy). J. Geochem. Explor. 200, 181–192. https://doi.org/10.1016/j.gexplo.2019.02.007.
Shepard, D., 1968. A two-dimensional interpolation function for irregularly-spaced data. In: Proceedings of the 1968 23rd ACM National Conference, ACM '68. Association for Computing Machinery, New York, NY, USA, pp. 517–524. https://doi.org/10.1145/800186.810616.
Shepard, D.S., 1984. Computer mapping: the SYMAP interpolation algorithm. In: Gaile, G.L., Willmott, C.J. (Eds.), Spatial Statistics and Models. Springer, Netherlands, Dordrecht, pp. 133–145. https://doi.org/10.1007/978-94-017-3048-8_7.
Smirnov, N., 1948. Table for estimating the goodness of fit of empirical distributions. Ann. Math. Stat. 19 (2), 279–281. https://doi.org/10.1214/aoms/1177730256.
Spoelstra, J., Leal, K.A., Senger, N.D., Schiff, S.L., Post, R., 2021. Isotopic characterization of sulfate in a shallow aquifer impacted by agricultural fertilizer. Groundwater 59, 658–670. https://doi.org/10.1111/gwat.13093.
Stevenazzi, S., Camera, C.A.S., Masetti, M., Azzoni, R.S., Ferrari, E.S., Tiepolo, M., 2020. Atmospheric nitrogen depositions in a highly human-impacted area. Water, Air, Soil Pollut. 231, 276. https://doi.org/10.1007/s11270-020-04613-y.
Stevenazzi, S., Zuffetti, C., Camera, C.A.S., Lucchelli, A., Beretta, G.P., Bersezio, R., Masetti, M., 2023. Hydrogeological characteristics and water availability in the mountainous aquifer systems of Italian Central Alps: a regional scale approach. J. Environ. Manag. 340, 117958. https://doi.org/10.1016/j.jenvman.2023.117958.
Stiff, H.A., 1951. The interpretation of chemical water analysis by means of patterns. J. Petrol. Technol. 3 (10), 15, 13.
Sutton, M.A., Howard, C.M., Erisman, J.W., Billen, G., Bleeker, A., Grennfelt, P., van Grinsven, H., Grizzetti, B. (Eds.), 2011. The European Nitrogen Assessment: Sources, Effects and Policy Perspectives. Cambridge University Press, Cambridge. https://doi.org/10.1017/CBO9780511976988.
Szocs, T., Rman, N., Süveges, M., Palcsu, L., Tóth, G., Lapanje, A., 2013. The application of isotope and chemical analyses in managing transboundary groundwater resources. Appl. Geochem., Spec. Issue Devoted 9th Int. Symp. Appl. Isotope Geochem. (AIG9) 32, 95–107. https://doi.org/10.1016/j.apgeochem.2012.10.006. Tarragona, Spain, September 2011.
Tiwari, A.K., Pisciotta, A., De Maio, M., 2019. Evaluation of groundwater salinization and pollution level on Favignana Island, Italy. Environ. Pollut. 249, 969–981. https://doi.org/10.1016/j.envpol.2019.03.016.
Tziritis, E., Sachsamanoglou, E., Güler, C., 2024. Evaluating spatiotemporal groundwater quality changes in the Rhodope coastal aquifer system (NE Greece) employing a GIS-assisted hybrid approach of multivariate statistics and inverse geochemical modeling. Sci. Total Environ. 947, 174676. https://doi.org/10.1016/j.scitotenv.2024.174676.
Ujević Bošnjak, M., Capak, K., Jazbec, A., Casiot, C., Sipos, L., Poljak, V., Dadić, Ž., 2012. Hydrochemical characterization of arsenic contaminated alluvial aquifers in Eastern Croatia using multivariate statistical techniques and arsenic risk assessment. Sci. Total Environ. 420, 100–110. https://doi.org/10.1016/j.scitotenv.2012.01.021.
Voudouris, K.S., Lambrakis, N.J., Papatheothorou, G., Daskalaki, P., 1997. An application of factor analysis for the study of the hydrogeological conditions in Plio-Pleistocene aquifers of NW Achaia (NW Peloponnesus, Greece). Math. Geol. 29, 43–59. https://doi.org/10.1007/BF02769619.
Voudouris, K., Panagopoulos, A., Koumantakis, J., 2000. Multivariate statistical analysis in the assessment of hydrochemistry of the northern korinthia prefecture alluvial aquifer system (Peloponnese, Greece). Nat. Resour. Res. 9, 135–146. https://doi.org/10.1023/A:1010195410646.
Wada, Y., Heinrich, L., 2013. Assessment of transboundary aquifers of the world—vulnerability arising from human water use. Environ. Res. Lett. 8, 024003. https://doi.org/10.1088/1748-9326/8/2/024003.
Yang, F., Liu, S., Jia, C., Gao, M., Chang, W., Wang, Y., 2021. Hydrochemical characteristics and functions of groundwater in southern Laizhou Bay based on the multivariate statistical analysis approach. Estuar. Coast Shelf Sci. 250, 107153. https://doi.org/10.1016/j.ecss.2020.107153.
Yang, J., Liu, H., Tang, Z., Peeters, L., Ye, M., 2022. Visualization of aqueous geochemical data using Python and WQChartPy. Groundwater 60, 555–564. https://doi.org/10.1111/gwat.13185.